6

Oligonucleotide conjugation to Tat peptide *via* gold nanoparticles

6.1 Introduction

Drawing on the difficulties in obtaining a labelled oligonucleotide peptide conjugate for cell studies *via* Diels-Alder methodology, as reported previously, it was decided to attempt an alternative approach to conjugation; linking the biomolecules *via* gold nanoparticles.

Gold nanoparticles (AuNPs) have been reported for use in a number of biological applications including labelling and biosensor applications, as delivery vehicles and as heat sources for imaging and tissue studies. [(1)] Notable amongst these reports of the biological function of AuNPs is their cellular uptake properties; they have been shown by imaging techniques to be localised [(2)] within vesicular compartments [(3)] in the cytoplasm of cells. Translocation of AuNPs into the intracellular environment brings about the inevitable question of biocompatibility, however cytotoxicity studies to date have shown no detrimental effects on cellular function after incubation with AuNPs of a variety of shapes and sizes [(3), (4).] Based on these observations it was concluded that AuNPs would be suitable for heterofunctionalisation with both oligonucleotides and Tat peptide as an alternative bioconjugation approach to Diels-Alder cycloaddition.

6.1.1 Properties of gold nanoparticles

Colloidal AuNPs were first reported by Faraday in 1857. [5] In his lecture to the Royal Society he describes the reduction of a dilute, aqueous solution of gold chloride by phosphorous, in the presence of CS_2, to form a ruby-red fluid of fine gold particles. The characteristic red colour of gold colloids, containing particles of diameter less than 40 nm, is a result of a strong absorption band in the UV-visible region, around 520 nm. This absorption band arises when the incident photon frequency is in resonance with the collective excitation of the conduction electrons (surface plasmons), leading the gold particles to exhibit absorptions with large molar extinction coefficients (in the region of ~ 3 x 10^{11} M^{-1} cm^{-1}). [6] This phenomenon was rationalised in a key publication by Mie in 1908. [7] Mie's theory states that the extinction of AuNPs is dependent on nanosphere radius and dielectric constant; increasing AuNP size led to a change in colloidal colour from deep red towards a less intense, blue-violet, resultant of a red-shift in surface plasmon resonance (SPR) towards longer wavelengths, caused by larger particles having greater ability to reflect light. This was later confirmed experimentally by Turkevitch and Garton. [8] Mie theory also states that optical extinction of AuNPs is dependent on the dielectric constant of the medium in which the nanoparticles are contained. Changes in the environment surrounding AuNPs lead to changes in the dielectric constant of the surrounding medium, in turn leading to shifts in plasmon resonance. This observation been manipulated for biosensing purposes; in intraparticle SPR, binding of a biomolecule to receptor functionalised AuNPs leads to a red-shift in the resonance wavelength. [9]

Aggregation of AuNPs also leads to observational changes in plasmon resonance. In interparticle SPR, aggregation leads to a large change in the dielectric constant of the individual nanospheres, brought about by the close proximity of the electromagnetic fields of neighbouring nanospheres. This is observed as a red-shift in plasmon resonance, giving rise to a broad extinction band at higher wavelengths (> 600 nm), accompanied by a change in colloidal colour from red to blue. This property of AuNPs has been used in a biosensing capacity, by conjugation of

receptor and target molecules to nanoparticles which, on binding, induce nanoparticle aggregation which can be detected colorimetrically. [1]

6.1.2 Synthesis and ligand functionalisation of gold nanoparticles

The synthesis of AuNPs in aqueous solution with diameters ranging from a few nanometers up to hundreds of nanometers is well documented. In a typical procedure, chloroaurate is reduced by citric acid, [10] bringing about nucleation of the Au (+3) ions in to form Au (0) nanoparticles. Nanoparticle size can be pre-selected and controlled by variation in the citrate-to-gold ratio. [11] In this type of synthesis, citric acid also acts as a ligand to stabilise the nanoparticles; the citrate ions are adsorbed onto the gold surface and, by virtue of their equal negative charges, repel each other, inducing stability to the colloidal dispersion. Disruption of this citrate layer, for example by addition of salts, results in aggregation to form larger, insoluble particulates.

Functionalisation of AuNPs can be achieved through manipulation of the outer shell of stabilising molecules; either by direct linkage of a ligand to the stabilising molecules, or by their replacement with a ligand in a ligand exchange reaction (**Fig. 6.1).**

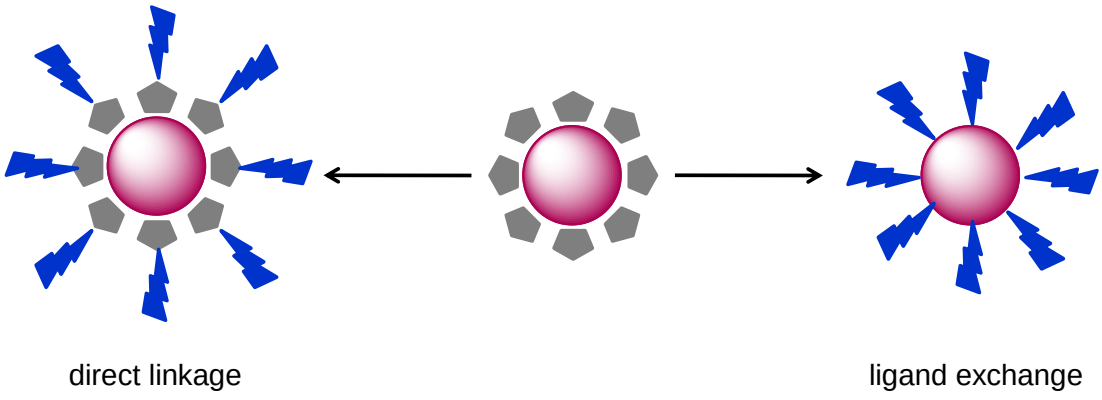

Figure 6.1 – *Schematic showing ligand functionalisation of stabilised colloidal AuNPs by direct linkage and by ligand exchange*

In selecting suitable ligands for gold nanoparticle functionalisation, the high affinity of thiols for gold surfaces is often employed. The use of alkanethiols has been reported for the arrangement of dense, ordered, self-assembled monolayers on gold surfaces, by the formation of Au-sulphur bonds. [12]

Functionalisation of AuNPs with alkanethiols is often achieved by way of reduction of gold salts in the presence of alkane thiols in a two-phase liquid-liquid system, and results in formation of AuNPs suitable for use in organic solvents. [13] Incorporation of different reactive groups into the alkanethiol ligands presents the opportunity for further functionalisation of AuNPs by reaction, post-monolayer assembly, with the desired moiety. [14] For functionalised AuNPs that can be applied in an aqueous environment, for example for conjugation to biomolecules, thiol ligands with carboxylic acids attached to the opposite end of the ligand, pointing into the colloidal solution, can be used; [15], [16] the charged carboxyl groups providing colloidal stability in the aqueous medium. These acid functionalities have the added advantage of being available for participation in bioconjugation reactions with amino groups, common to many biomolecules. Further stabilisation of functionalised nanoparticles in aqueous media has been reported, with the incorporation of poly(ethyleneglycol) (PEG) chains into ligands. [17], [18], [19], [20] These types of ligand induce increased colloidal stability by provision of a strongly bound, extremely hydrophilic, yet uncharged shell around the nanoparticles which, even under conditions of high pH and ionic strength, do not aggregate. PEGylated ligands have been reported for conjugation of AuNPs, in aqueous media, to biomolecules such as proteins [21], [22] and antibodies. [23]

6.1.3 Oligonucleotide functionalisation of gold nanoparticles

The first reports of gold nanoparticle functionalisation with oligonucleotides were published simultaneously. Both papers described the manipulation of Watson-Crick base pairing as a method for the controlled assembly of gold nanostructures, by hybridisation of AuNPs functionalised with sequences of single-stranded DNA to a DNA template (**Fig. 6.2**). [24], [25]

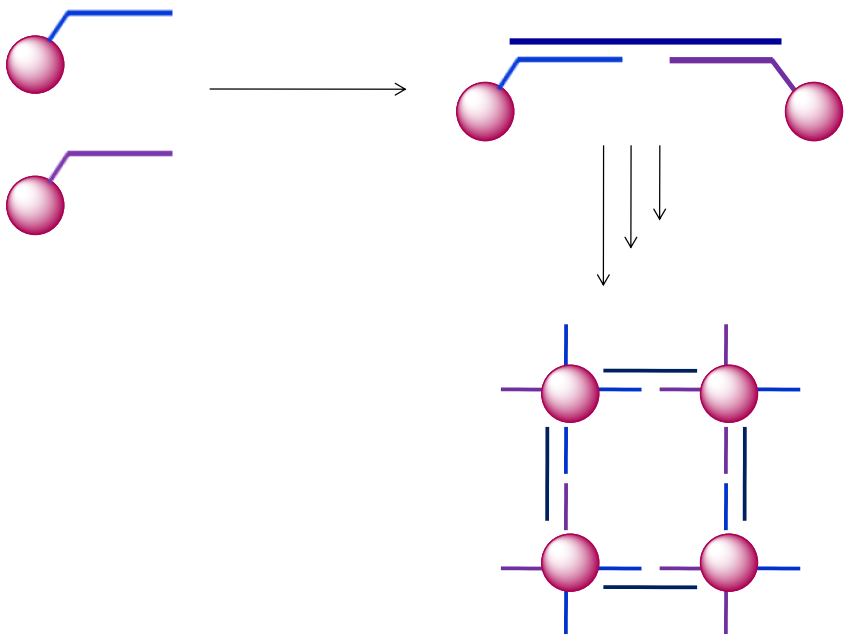

Figure 6.2 – *Schematic showing controlled gold nanostructure assembly through hybridisation of AuNPs functionalised with single-stranded DNA to a DNA template*

Alivistatos *et al.* describe the synthesis of gold nanoparticle clusters, passivated with water-soluble phosphine ligands and containing one *N*- propylmaleimide substituent per cluster. This linker molecule was used for oligonucleotide functionalisation by way of selective coupling to a sulfydryl group incorporated into either the 3'- or the 5'- termini of the selected oligonucleotide sequence. Meanwhile Mirkin *et al.* report a more simplistic approach to nanoparticle functionalisation, taking advantage of the affinity of thiols for gold surfaces. Citrate-reduced AuNPs were conjugated to oligonucleotide sequences modified at the 3'-terminus with alkane thiols. Notable in this report was the observation that oligonucleotide functionalised gold colloid was found to be more stable than bare gold. On exposure to increased temperature and salt concentration, bare nanoparticles aggregated irreversibly while oligonucleotide functionalised nanoparticles exposed to the same conditions remained stable. The authors proposed that the DNA-modified surfaces prevent the particles becoming close enough to result in particle growth.

The incidence of hybridisation of oligonucleotide functionalised AuNPs to form larger nanoparticle particulates was quickly manipulated for use as an oligonucleotide detection method. [26] The larger gold particle clusters formed post-hybridisation bring about a shift in surface plasmon resonance that in turn leads to a

change in colloidal colour from red to blue. Elghanian *et al.* found that this phenomenon could be easily visualised by spotting hybridisation solutions on a solid support. A positive result led to observation of a blue spot; a negative result led to observation of a red spot. As such, the authors were able to report detection of single base mismatches and single base deletions in oligonucleotide sequences at concentrations as low as femtomolar. A further key development in this study was the reported protocol for oligonucleotide conjugation to AuNPs. Increased oligonucleotide surface coverage was achieved by adding 5'- or 3'- thiolated oligonucleotides to AuNPs, followed by a 'salt aging' process, whereby NaCl concentration is increased incrementally. This increases oligonucleotide surface coverage by weakening the electrostatic interactions between the negatively charged phosphate groups along the oligonucleotide backbone and the positively charged gold nanoparticle surfaces, thereby increasing the surface area available for adsorption to the oligonucleotide thiol groups. This is now the standard protocol for gold nanoparticle functionalisation with thiolated oligonucleotides. [27]

More recent work on detection methods using oligonucleotide derivatised AuNPs has focused on the use of multi-thiol modified oligonucleotides for surface adsorption [28], [29], [30] Nanoparticles conjugated to monothiolated oligonucleotides have been found to have decreased stability under conditions of prolonged elevated temperatures, high NaCl concentrations and in biological buffers containing certain additives such as dithiothreitol (DTT) or mercaptoethanol. [29] These conditions bring about thiol desorption, leading to irreversible nanoparticle aggregation. The lability of monothiolated oligonucleotides conjugated to AuNPs has been quantified by fluorescence spectroscopy using labelled oligonucleotides. [31]

As such, the possibility of anchoring oligonucleotide sequences to AuNPs through more than one sulphur atom has been investigated. Oligonucleotides functionalised with a cyclic steroid dithiol, [28] thioctic acid [30] (also a cyclic dithiol) and a trihexylthiol group, [29] conjugated to AuNPs, have all been shown to increase colloidal stability on treatment with DTT. This is thought to be due, in part at least, to surface attachment of oligonucleotides through multiple sulphur atoms. Of particular interest amongst these multi-thiol groups is thioctic acid, which is simple in structure, inexpensive and commercially available.

6.1.4 Tat peptide functionalisation of gold nanoparticles

There are several reports in the literature of the functionalisation of different types of nanoparticles with Tat peptide derived sequences. [32], [33], [34], [35] Patel *et al.* describe functionalisation of AuNPs with a mixed monolayer of thiol modified DNA and cysteine modified Tat peptide; [35] however the majority of these reports describe surface attachment of the peptide moiety *via* a covalent linkage. Particularly notable amongst these reports is an account, by de la Fuente and Berry of the functionalisation of AuNPs with Tat peptide in this way. [33] In a two-phase approach, $HAuCl_4$ was first surface-derived with the non-amino acid tiopronin, followed by reduction with $NaBH_4$ to form tiopronin functionalised AuNPs (**Scheme 6.3**). It was then possible to react the free carboxyl groups of the tiopronin molecules, using carbodiimide chemistry, with amino groups on the peptide side chain residues, for bioconjugation of the AuNPs to Tat peptide.

The Tat peptide functionalised nanoparticles were tested for their biocompatibility then shown, by TEM imaging, to penetrate human fibroblasts and accumulate in the cell nucleus. Significant in this report is the observation that, despite the involvement of the peptide's amino side chains in covalent linkage to the nanoparticles, the peptide nanoparticle conjugates were still able to penetrate fibroblast cell membranes; this is interesting, considering the implication of the amino side chains in the cellular uptake mechanism for Tat peptide. [36], [37]

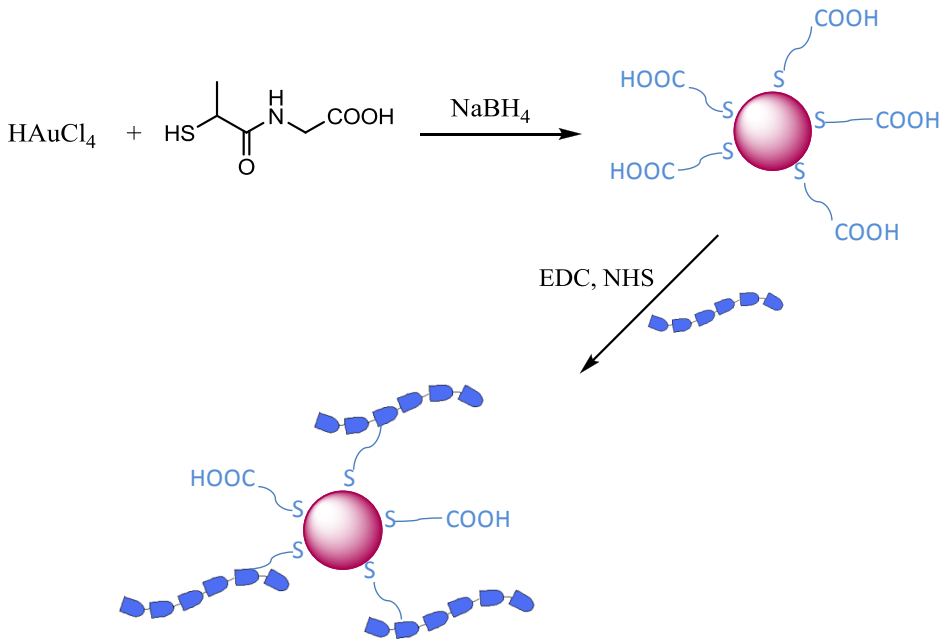

Scheme 6.3 – *Tat peptide bioconjugation to tiopronin functionalised AuNPs by amide coupling to the amino side chain residues* [33]

6.2 Results and discussion

6.2.1 Bioconjugation of Tat peptide to gold nanoparticles

In the first step towards oligonucleotide conjugation to Tat peptide *via* AuNPs, functionalisation of AuNPs with Tat peptide was optimised. Prior to publication of the report by Patel *et al.* [35] on synthesis of DNA peptide nanoparticle conjugates through formation of a mixed monolayer of DNA and Tat peptide, functionalisation of AuNPs with Tat peptide derived sequence (**1**), modified with a cysteine residue at the *N*- terminus, was attempted.

Peptide sequence 1 : CYGRKKRRQRRR

Peptide sequence (**1**) was added directly to AuNPs in phosphate buffer (pH 7.6). Use of phosphate buffer containing 0.1 M NaCl, for screening the electrostatic interactions between the largely cationic peptide and the stabilising, anionic citrate

layer surrounding the nanoparticles, was attempted first; however this induced nanoparticle aggregation. The peptide was added to nanoparticles, in phosphate buffer only, in incremental amounts of decreasing peptide. At 10^{-5} M and 10^{-6} M concentration of peptide in the colloidal suspension, nanoparticle aggregation was immediately visible; to the naked eye, by an immediate change in colloidal colour from red to blue (**Fig. 6.4**) and by a red-shift in the surface plasmon from 521 nm to over 600 nm. (**Fig. 6.5** – blue traces). This was quickly followed by complete colloidal coagulation to form insoluble, black particulates.

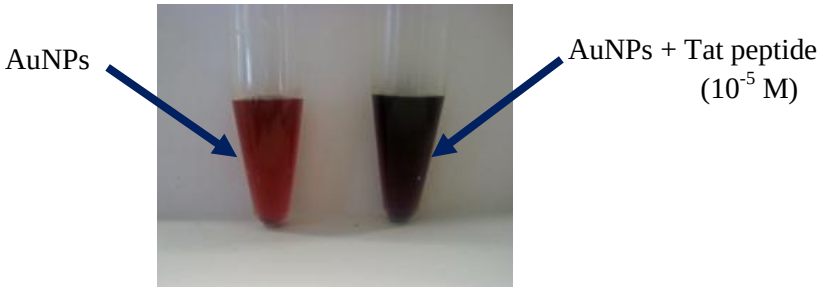

Figure 6.4 – *Image showing gold colloid aggregation observed on addition of Tat-SH, indicated by colour change from wine-red to blue.*

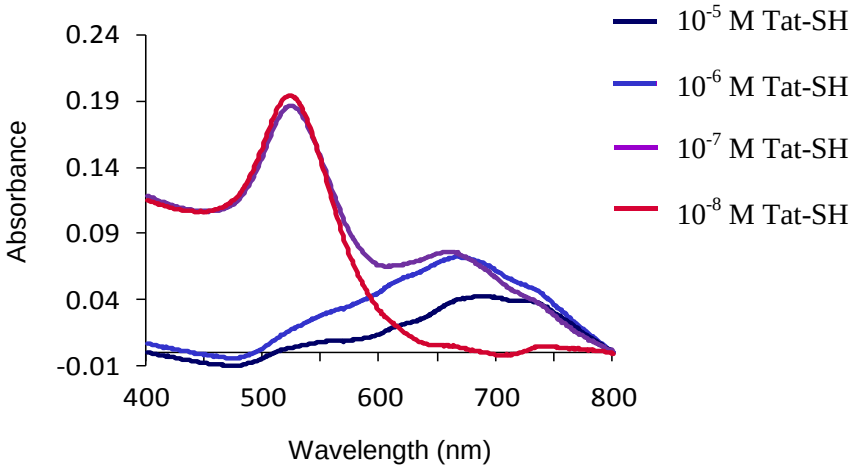

Figure 6.5 – *UV-vis spectrum showing gold colloid aggregation observed (indicated by a red-shift from 521 nm to over 600 nm) as a function of Tat-SH concentration.*

At 10^{-7} M peptide, partial aggregation was observed. Only as low as 10^{-8} M peptide was no aggregation induced (**Fig. 6.5** – pink spectrum). However, at this concentration the number of peptide molecules per nanoparticle was equivalent to a maximum value of approximately 0.5. This level of Tat peptide surface coverage was deemed too low to be viable for synthesis of an oligonucleotide Tat peptide conjugate with cell penetrating abilities.

It was clear that direct addition of the highly cationic Tat peptide to AuNPs was to the detriment of colloidal stability; this is likely to be due to neutralisation of the stabilising negative charges of the citrate layer. As such, an alternative approach was required. Tshikhudo *et al*. [38] report the design of a thiolalkylated PEG ligand suitable for use in the formation of stable, water soluble, bioavailable AuNPs (**Fig. 6.6**). The ligand incorporates a thiol group at one end for surface attachment to AuNPs, a hydrophobic alkane chain for increased stability of the self-assembled monolayer, a highly hydrophilic PEG chain to promote water solubility and thereby nanoparticle biocompatibility and a reactive 'R' group for biomolecule attachment through a covalent linkage.

Based on this design, a ligand for covalent attachment of Tat peptide to AuNPs was proposed (**Fig. 6.7**). This ligand is derived from thioctic acid which incorporates both a disulfide moiety for stronger adsorption to gold surfaces and a hydrophobic component for enhanced stability of the self-assembled monolayer. Thioctic acid is linked to a hydrophilic PEG chain, which can be varied in length, to impart water solubility to the functionalised nanoparticles. The PEG component of the ligand is also modified with a carboxylic acid for conjugation of the ligand to Tat peptide, by coupling to the amino groups on the peptide residues. This should be at no cost to the cellular uptake of the peptide, as reported previously by de la Fuente. [33]

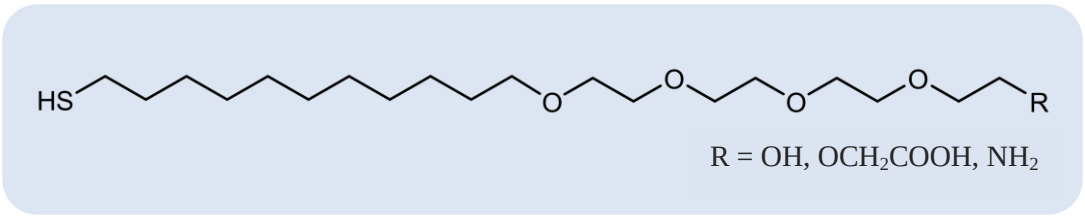

Figure 6.6 – *Thiolalkylated PEG ligand reported by Tshikhudo et. al* (38) *for use in the formation of stable, water soluble, bioavailable AuNPs*

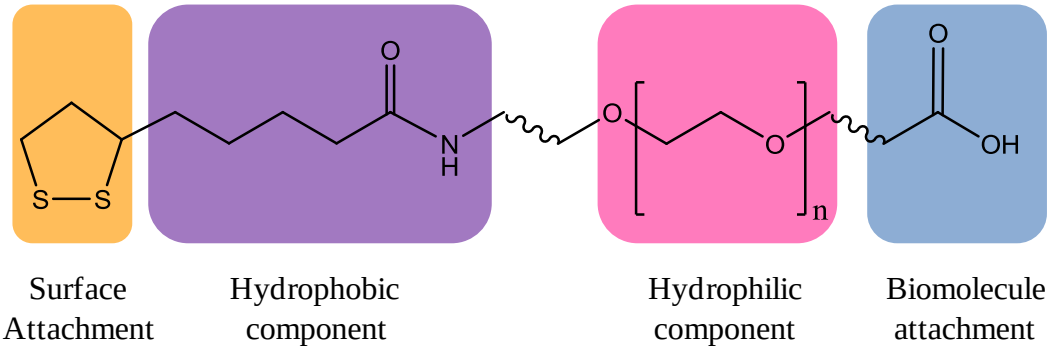

Figure 6.7 – *Proposed design of a PEGylated ligand for stable bioconjugation of Tat peptide to AuNPs.*

6.2.1.1 Ligand synthesis

Two ligand molecule were synthesised for use in the functionalisation of AuNPs with Tat peptide; one incorporating three PEG units ($(PEG)_3$), and one incorporating forty one PEG units ($(PEG)_{41}$). The two ligands were compared in terms of their stabilising influence on the introduction of Tat peptide to colloidal AuNPs.

Synthesis of a $(PEG)_3$ ligand was based around a commercially available compound, *tert*-butyl 12-amino-4, 7, 10-trioxadodecanoate (**1**) (Sigma-Aldrich). This molecule contains an amino functionality suitable for amide coupling with thioctic acid, for incorporation of the surface attachment component of the ligand and, on removal of the *tert*-butyl protecting group, a carboxylic acid functionality for bioconjugation to Tat peptide. However, this molecule was costly to purchase from a commercial source so it was decided to attempt its synthesis from less expensive starting materials in-house (**Scheme 6.4**).

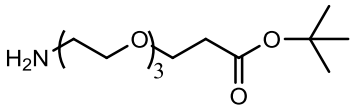

1

The first step in the synthesis of (**1**) was modification of the PEG component of the ligand to include a carboxylic acid functionality, by reaction of three equivalents of triethylene glycol with *tert*-butyl acrylate in THF, using a catalytic amount of sodium metal, to afford (**2**). [39] Greater than quantitative yield (111 %) was observed for this reaction but, on examination of the ^{1}H NMR, this was attributed to excess triethylene glycol. A Mitsunobu reaction, using phthalimide, was then performed in the first step of conversion of the terminal hydroxyl functionality of (**2**) to an amino functionality, generating protected amine (**3**) in moderate yield (49 %). Cleavage of the phthalimide protecting group was achieved by treatment of (**3**) with hydrazine monohydrate to afford PEGylated amine (**1**). Using the method depicted (**Scheme 6.4**), over 1 gram of (**1**) was synthesised at little expense.

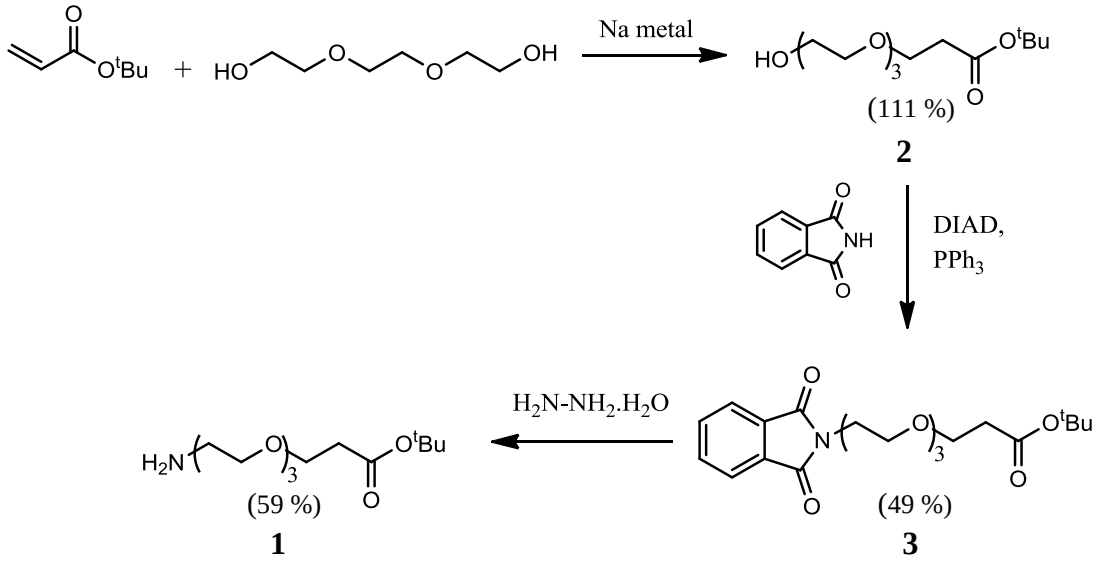

Scheme 6.4 – *Approach to in-house synthesis of commercially available tert-butyl 12-amino-4, 7, 10-trioxadodecanoate* ***(1)***

The final steps in the manufacture of a $(PEG)_3$ ligand, according to the design detailed in **Figure 6.7**, were attachment of the disulfide component for gold surface attachment, followed by cleavage of the *tert*-butyl group to liberate the carboxylic acid functionality (**Scheme 6.5**). The amino terminus of (**1**) was first coupled with thioctic acid, using carbodiimide chemistry, to afford disulfide (**4**). DIC was the coupling agent of choice as the diisopropylurea by-product would be much easier to remove than the dicyclohexylurea by-product generated by use of the, often more common choice of coupling agent, DCC.

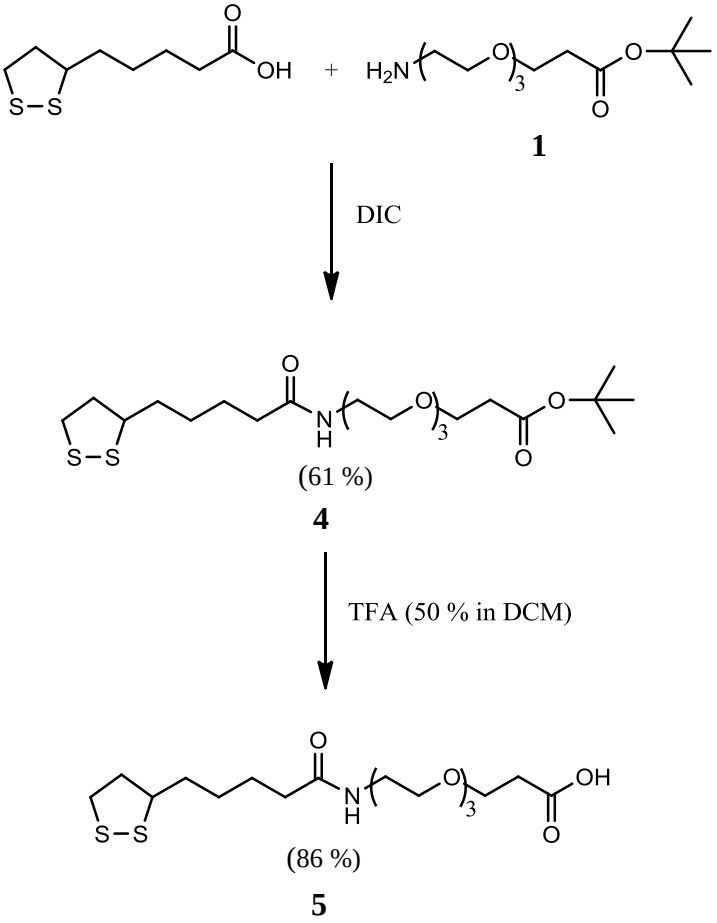

Scheme 6.5 – *Attachment of disulfide component for synthesis of $(PEG)_3$ ligand*

It should be noted that care had to be taken in solvent removal during work up and purification of this reaction; under reduced pressure, at temperatures greater than 30 ^{o}C, polymerisation of the disulfide was observed as the formation of a sticky, insoluble yellow solid. Cleavage of the *tert*-butyl protecting group was achieved *via* treatment of (**4**) with TFA (**Scheme 6.5**) to afford the desired ligand (**5**). To ensure removal of all excess acid, a solution of (**5**) was stirred with morpholinomethyl polystyrene beads, [40] which were then removed by filtration, before addition to AuNPs.

It was noted that, in the synthesis of the $(PEG)_3$ ligand, a highly polar eluent system was required for purification by column chromatography of intermediate (**4**) (see 6.4.2 – *Chemical Synthesis* for details). This was attributed to its highly polar nature, imparted by the PEG chain. From this observation it was deemed that, for synthesis of a $(PEG)_{41}$ ligand whereby the PEG chain is extensively increased in length, solution phase chemistry, using column chromatography for purification, would not be viable.

As such, a solid-phase synthesis approach was taken (**Scheme 6.6**). This allows for purification at each step by thorough washing of the functionalised resin to remove by-products and excess reagents.

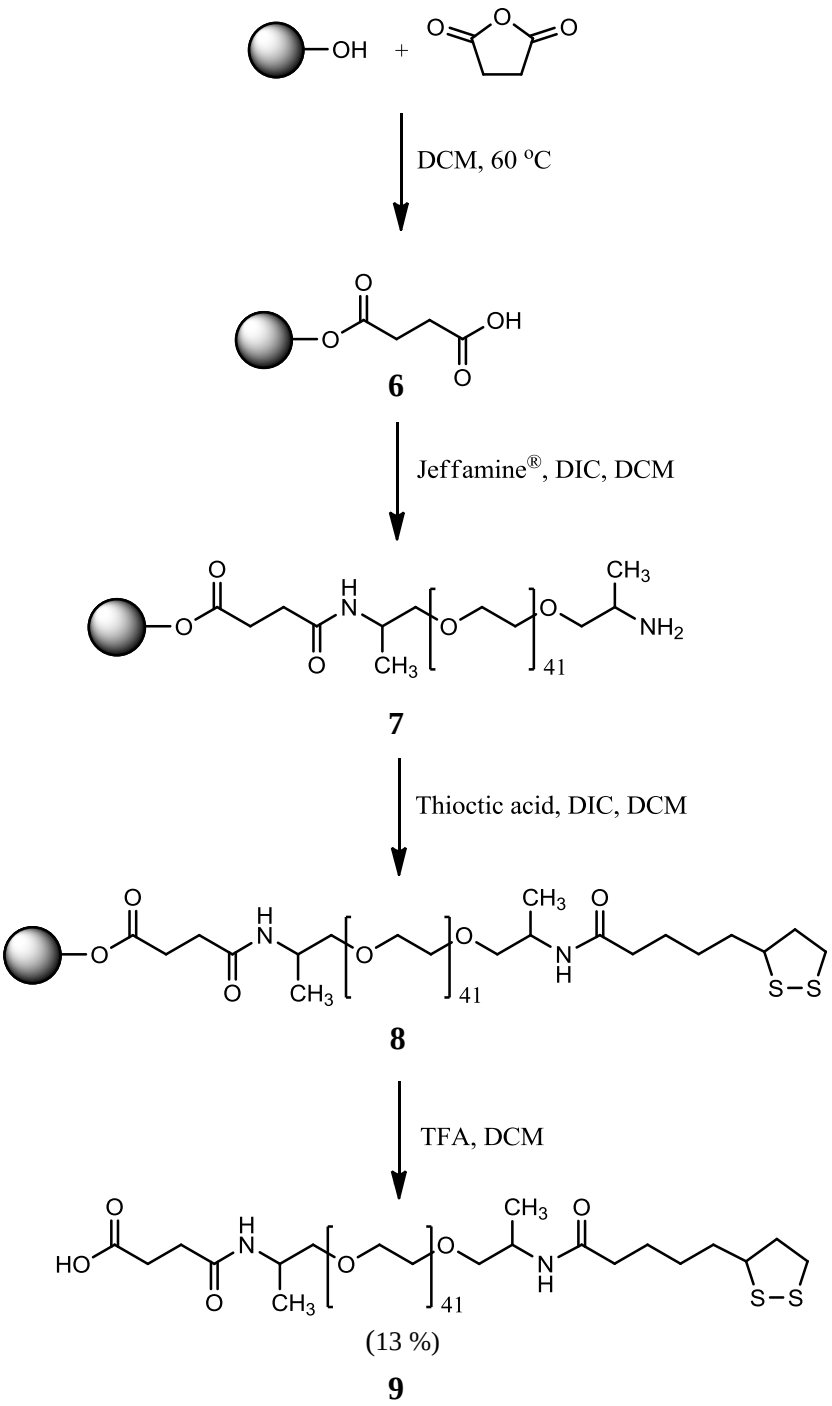

Scheme 6.6 – *Solid-phase synthesis of $(PEG)_{41}$ ligand*

Wang resin was selected as the solid support for use in synthesis of $(PEG)_{41}$ ligand (**9**).

In the first step of the synthesis a ring opening reaction was performed, heating Wang resin to reflux with excess succinic anhydride in DCM, to generate acid

functionalised resin (**6**). Functionalising the resin in this way affords a carboxylic acid through which the next building block in the ligand can be attached, but also means that after construction of the rest of the ligand, cleavage from the resin will result in ligand functionalisation with a carboxylic acid at one end for biomolecule attachment, as per the design shown in **Figure 6.7**, earlier. Success of reaction of the resin with succinic anhydride was measured by performing a test with malachite green oxalate, [40] which shows a positive result for COOH-functionalised resins.

Incorporation of the hydrophilic, PEG component of the ligand was achieved by reaction of the acid-functionalised resin with Jeffamine® diamine – a commercially available polymer containing approximately forty one PEG units – to afford amino-functionalised resin intermediate (**7**). Carbodiimide chemistry, using coupling agent DIC, was adopted for this reaction. Success of the reaction was measured by performing a TNBS test, [40] which shows a positive result for amino-functionalised resins.

The penultimate step in the synthesis of a $(PEG)_{41}$ ligand was incorporation of the surface attachment component. This was accomplished, as per synthesis of the $(PEG)_3$ ligand, by amide formation with thioctic acid, once again using coupling agent DIC, to afford disulfide-functionalised resin intermediate (**8**). Generation of the desired $(PEG)_{41}$ ligand (**9**) was then achieved by cleavage from the resin, by treatment of (**8**) with TFA. Ligand (**9**) took the form of a viscous oil, making it possible to remove excess TFA simply by washing with diethyl ether. The overall yield of this synthesis was low (13 %), however, since only very small quantities of the ligand would be required for functionalisation of AuNPs, this did not present a problem. Successful synthesis of the $(PEG)_{41}$ ligand was confirmed by MALDI-TOF mass spectrometry. The approximate calculated mass of the polymer was 2188. The mass found was 2086.6 ± 346.9.

6.2.1.2 Ligand functionalisation of gold nanoparticles

The initial step in conjugation of Tat peptide to AuNPs was functionalisation of the nanoparticles with PEGylated ligands (**5**) and (**9**) by adsorption to the gold surfaces through the ligands' cyclic disulfide components. AuNPs were incubated overnight with excess ligand in an attempt to achieve maximum surface coverage. Separation

of the ligand modified nanoparticles from the excess ligand was easily achieved, by centrifugation. Colloidal gold dispersions are such that, on centrifugation, the nanoparticles are concentrated to a small red pellet, allowing for easy removal of the clear supernatant solution containing any ligand that has not attached to the gold surfaces. The nanoparticles can then be easily resuspended in fresh buffer. This washing process can be repeated several times to ensure complete extraction of the nanoparticles from excess reagents.

On addition of the $(PEG)_3$ ligand (**5**) to AuNPs to generate ligand functionalised nanoparticles, herein known as $(PEG)_3$@AuNPs, a darkening in colloidal colour, from ruby-red to wine-red, was observed (**Fig. 6.8 A**). On examination of the $(PEG)_3$@AuNPs by UV-vis spectroscopy, a shift in λ_{max} from 521 nm to 527 nm, on comparison with bare AuNPs, was observed (**Fig. 6.8 B**). This red-shift in the surface plasmon of the AuNPs is taken to be evidence of successful modification of the nanoparticles with the ligand, with the change in surrounding environment bringing about a change in nanoparticle plasmonics.

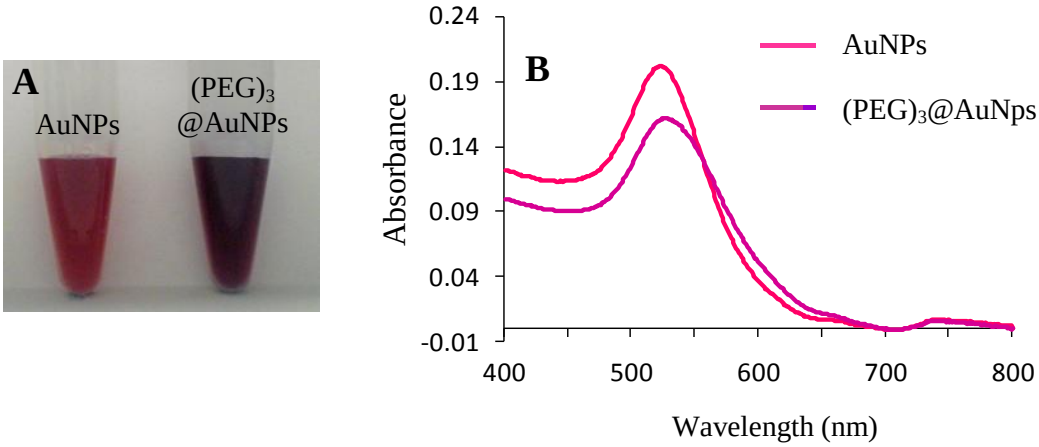

Figure 6.8 – **A** *Image showing gold colloid colour change from red to wine-red on addition of* $(PEG)_3$ *ligand;* **B** *UV-vis spectra of gold colloid showing red-shift from 521 nm to 527 nm on addition of* $(PEG)_3$ *ligand*

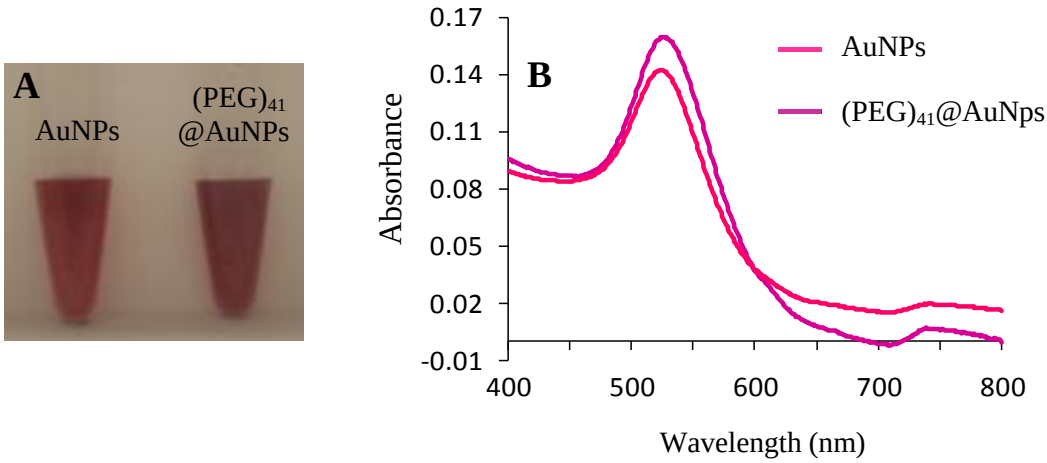

Figure 6.9 – **A** *Image showing no gold colloid colour change on addition of* $(PEG)_{41}$ *ligand;* **B** *UV-vis spectra of gold colloid showing smaller red-shift from 522 nm to 526 nm on addition of* $(PEG)_{41}$ *ligand c.f.,* $(PEG)_3$ *ligand*

On addition of the $(PEG)_{41}$ ligand (**9**) to AuNPs to generate ligand functionalised nanoparticles, herein known as $(PEG)_{41}$@AuNPs, no change in colloidal colour was visible to the naked eye (**Fig. 6.9 A**). However, a similar, albeit smaller, red-shift in λ_{max} from 522 nm to 526 nm of the PEG_{41}@AuNPs compared to bare AuNPs, was still observed (**Fig. 6.9 B**). This is again indicative of successful binding of the ligand to the nanoparticles; however the smaller red-shift also shows increased stability of $(PEG)_{41}$@AuNPs compared to $(PEG)_3$@AuNPs. This is thought to be due to the enhanced hydrophilicity of the $(PEG)_{41}$@AuNPs, generated by the increase in length of the PEG chain, leading to greater stability of the aqueous colloidal dispersion.

6.2.1.3 Tat peptide bioconjugation to ligand functionalised gold nanoparticles

After modification of the AuNPs with the PEGylated ligands, functionalisation with Tat peptide was achieved by coupling of the carboxylic acids of the ligand molecules to the amino groups of the peptide side chain residues, using aqueous carbodiimide chemistry (**Scheme 6.7**).

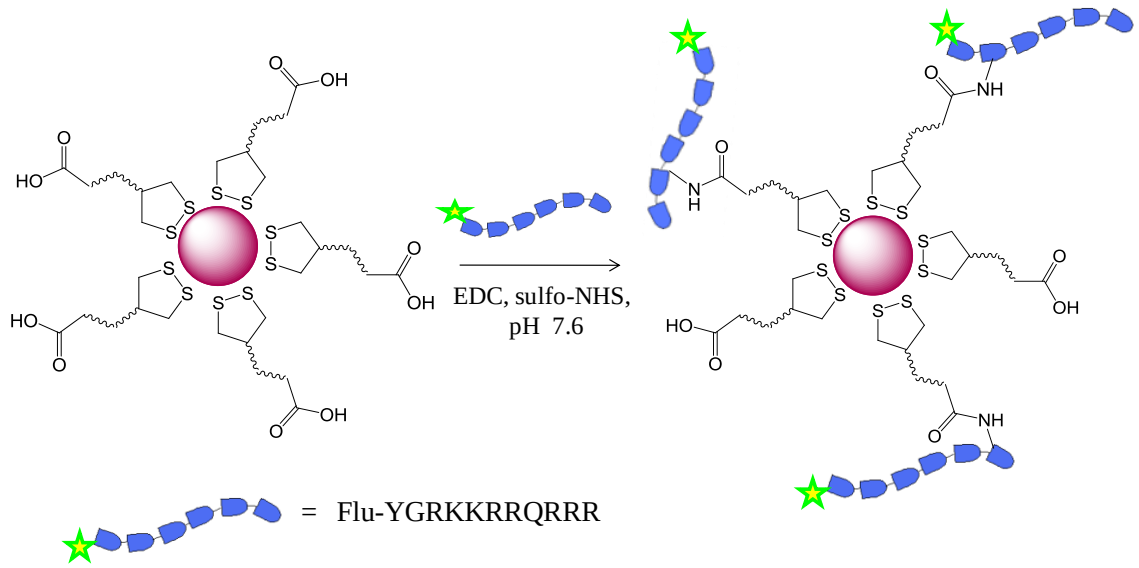

Scheme 6.7 – *Bioconjugation of Tat peptide to (PEG)$_n$@AuNPs by amide coupling, using carbodiimide chemistry to the peptide's amino side chain residues.*

For amide formation, the water-soluble carbodiimide EDC was used to form an active ester with the carboxyl groups of the PEG ligand. However, it is known that the *O*-acylisourea active ester formed by reaction with EDC is subject to rapid hydrolysis in aqueous solutions. [41] This is particularly problematic when solutions of the carboxylate are dilute, as is the case for the PEG carboxylate groups adsorbed onto AuNPs. The issue was overcome by use, in conjunction with EDC, of sulfo-NHS to form a water-soluble, succinimidyl ester intermediate with greater stability to hydrolysis; sulfo-NHS active esters have a half-life extending to hours [42] and have been shown to increase yields of amide couplings by up to 20 %. [43] Succinimidyl esters have been shown to react rapidly with amines in phosphate buffers at between pH 7 and 8 [44] so bioconjugation was performed mid-range, at pH 7.6. After incubating the ligand-functionalised nanoparticles for thirty minutes with EDC and sulfo-NHS, to allow for formation of the active ester, excess Tat peptide sequence (**2**) was added. Fluorescein modified Tat peptide was used to allow surface coverage quantification of the conjugated peptide, by fluorescence analysis (see 6.2.2 – *Quantification of Tat peptide conjugated to AuNPs*).

Peptide sequence 2: Fluorescein-YGRKKRRQRRR

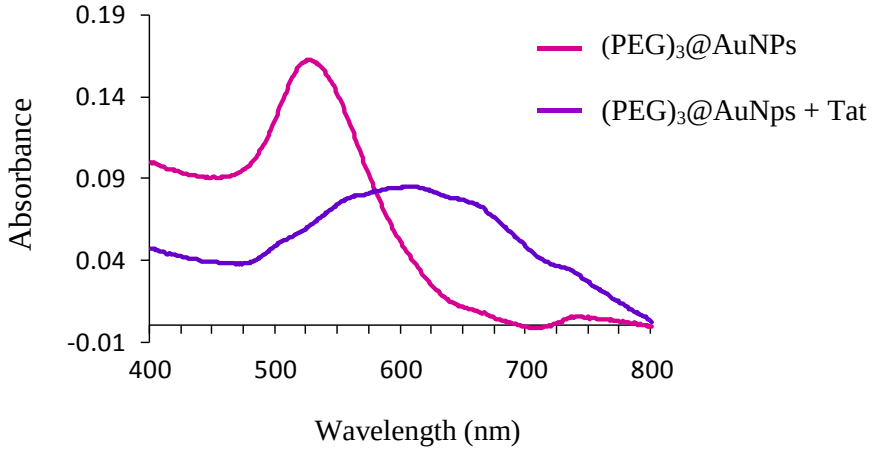

Figure 6.10 – *UV-vis spectra showing gold nanoparticle aggregation on addition of Tat peptide to (PEG)$_3$@AuNPs, as indicated by a red-shift in λ_{max} to over 600 nm*

On addition of Tat peptide to AuNPs functionalised with the activated $(PEG)_3$ ligand, aggregation was immediately observed, with a change in colloidal colour from red to blue and a red-shift in λ_{max} from 527 nm to 611 nm (**Fig. 6.10**). Aggregation of the nanoparticles quickly progressed to irreversible, resulting in precipitation of solid, black particulates.

However, on addition of the peptide to activated $(PEG)_{41}$@AuNPs, no change in colloidal colour, or shift in λ_{max} was observed (**Fig. 6.11**). This appears to be further evidence as to the stabilising effect of the long PEG chain of the $(PEG)_{41}$ ligand; this could be by way of the lengthy chains 'wrapping' themselves around the nanoparticles to which they are bound, thereby preventing aggregation.

The activated $(PEG)_{41}$@AuNPs were incubated with excess Tat peptide at room temperature, overnight. The nanoparticles were then washed, as described previously, to remove the excess peptide and coupling agents, affording peptide conjugated AuNPs, herein described as Tat@AuNPs.

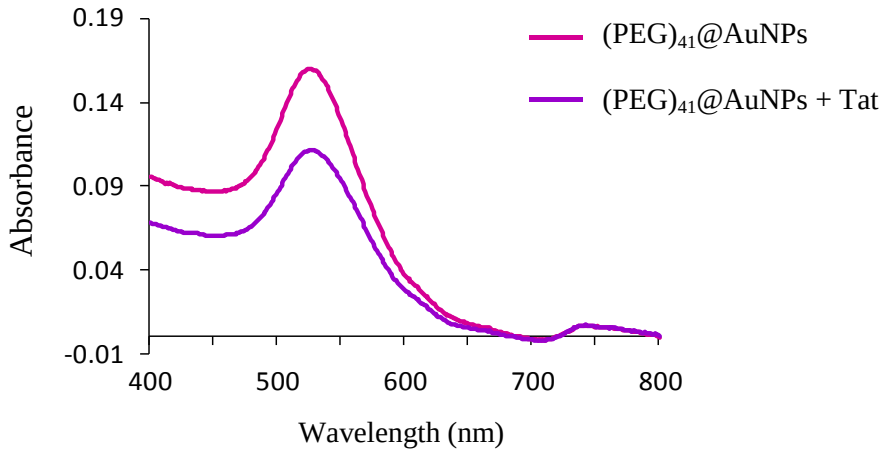

Figure 6.11 – *UV-vis spectra showing gold nanoparticle stability on addition of Tat peptide to (PEG)$_{41}$@AuNPs, as indicated by the absence of a red-shift in λ_{max}*

In order to prove the success of ligand functionalisation and the proceeding conjugation of Tat peptide to AuNPs, it was decided to measure the zeta potential of (PEG)$_{41}$@AuNPs and Tat@AuNPs. Zeta potential is the overall charge that a particle acquires in a specific medium. The size of the zeta potential indicates the stability of a colloidal system; particles having either a large positive or a large negative zeta potential will repel each other and the system will be stable. If a colloidal suspension has a low zeta potential there is little repulsion between particles, inducing instability in the dispersion which can lead to particle aggregation. Generally, values of +30 or -30 mV are indicative of a stable suspension; colloids with potentials lying on either side of these (i.e. greater than +30 mV or less than -30 mV) are regarded as stable.

In the case of the gold colloid used in this study, particle repulsion is brought about by the negatively charged citrate molecules adsorbed to the nanoparticles. It follows then that covalent attachment of the highly cationic Tat peptide sequence should result in an overall reduction in the size of the zeta potential of the colloidal suspension of Tat@AuNPs, compared to bare gold colloid (AuNPs).

The zeta potentials of bare colloid, (PEG)$_{41}$@AuNPs and Tat@AuNPs were measured, and analysed in conjunction with measurements obtained for the particle size of the functionalised gold colloids (**Table 6.1** and **Fig. 6.12**).

Nanoparticle functionalisation	Particle Size (nm)	Zeta Potential (mV)
AuNps	23.3	- 55.1
$(PEG)_{41}$@AuNPs	31.2	- 28.8
Tat@AuNps	36.3	- 22.3

Table 6.1 – *Particle size and zeta potential values for bare AuNPs and nanoparticles functionalised with $(PEG)_{41}$ ligand and Tat peptide*

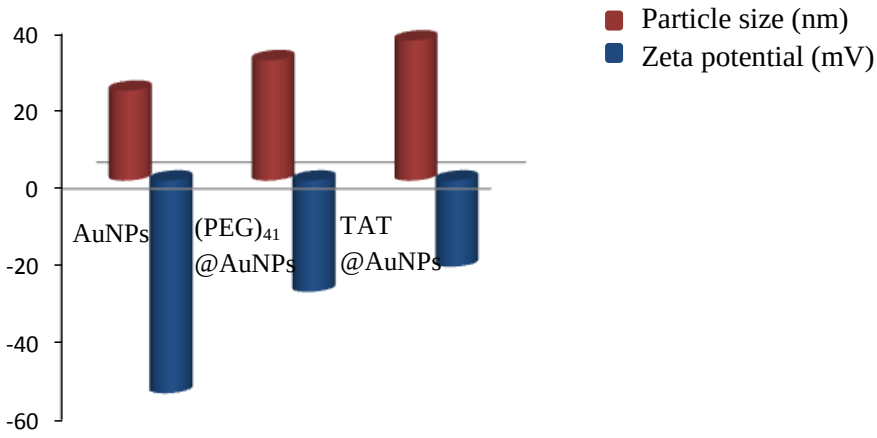

Figure 6.12 – *Graph showing comparison of particle size and zeta potential values for bare AuNPs and nanoparticles functionalised with $(PEG)_{41}$ ligand and Tat peptide*

On examination of the gathered data, it was found that functionalisation of AuNPs with the $(PEG)_{41}$ ligand resulted in an increase in colloidal zeta potential, compared with that of bare nanoparticles. This can be accounted for by the accompanying measured increase in particle size, equal to approximately 8 nm; while surface modification of the AuNPs with the disulfide ligand results in displacement of some of the anionic citrate residues, there remains stabilising anionic charge, attributed to the carboxyl functionalities of the surface-bound ligands. However, the increase in surface area of the $(PEG)_{41}$@AuNPs, owing to the long PEG chains of the $(PEG)_{41}$ ligand, results in an overall decrease in the surface area-to-charge ratio of the nanoparticles, thereby leading to the observed increase in zeta potential.

A further increase in zeta potential was observed on examination of Tat@AuNPs. This was to be expected, since functionalisation with the cationic peptide should

bring about an overall decrease in surface charge of the nanoparticle conjugates. In accordance with the increase in zeta potential, an increase in particle size, of approximately 5 nm, was also observed. This data was taken to be evidence that functionalisation of AuNPs with Tat peptide, by way of covalent attachment to surface-bound $(PEG)_{41}$ ligands, had been successfully accomplished.

6.2.2 Quantification of Tat peptide conjugated to gold nanoparticles

Whilst zeta potential and particle size data indicated that conjugation of Tat peptide to AuNPs had been accomplished, it was necessary to characterise the conjugates by quantification of the number of peptide molecules attached to the nanoparticle surfaces. This was achieved by functionalisation of nanoparticles with a fluorescently labelled Tat peptide derivative. Following bioconjugation and repeated washing of Tat@AuNPs to remove any unreacted peptide, the conjugated peptide was cleaved from the nanoparticle surfaces then quantified by fluorescence analysis. It is not possible to measure the fluorescence of the peptide functionalised colloid directly since AuNPs are known to be fluorescence quenchers.

This was first attempted by a displacement method, using dithiothreitol (DTT) [31]. This method relies on the competition of disulfide DTT with the disulfide functionalised linker molecule. The success of this method is usually indicated by aggregation of the nanoparticles in the conjugate buffer, and a red-shift in the surface plasmon towards 700 nm, as a result of the removal of the stabilising effect of the conjugated molecules and replacement with DTT. **Figure 6.13 A** shows an example of this, for treatment of thiol-DNA functionalised nanoparticles with 1M DTT. However, even addition of several aliquots of 1M DTT to the Tat peptide functionalised nanoparticles, and incubation overnight, did not induce nanoparticle aggregation. This is again evidence of the enhanced colloidal stability, brought about by functionalisation with the $(PEG)_{41}$ ligand. This is further supported by UV-vis spectroscopy data taken of Tat@AuNPs before, and after, addition of DTT (**Fig. 6.13 B**).

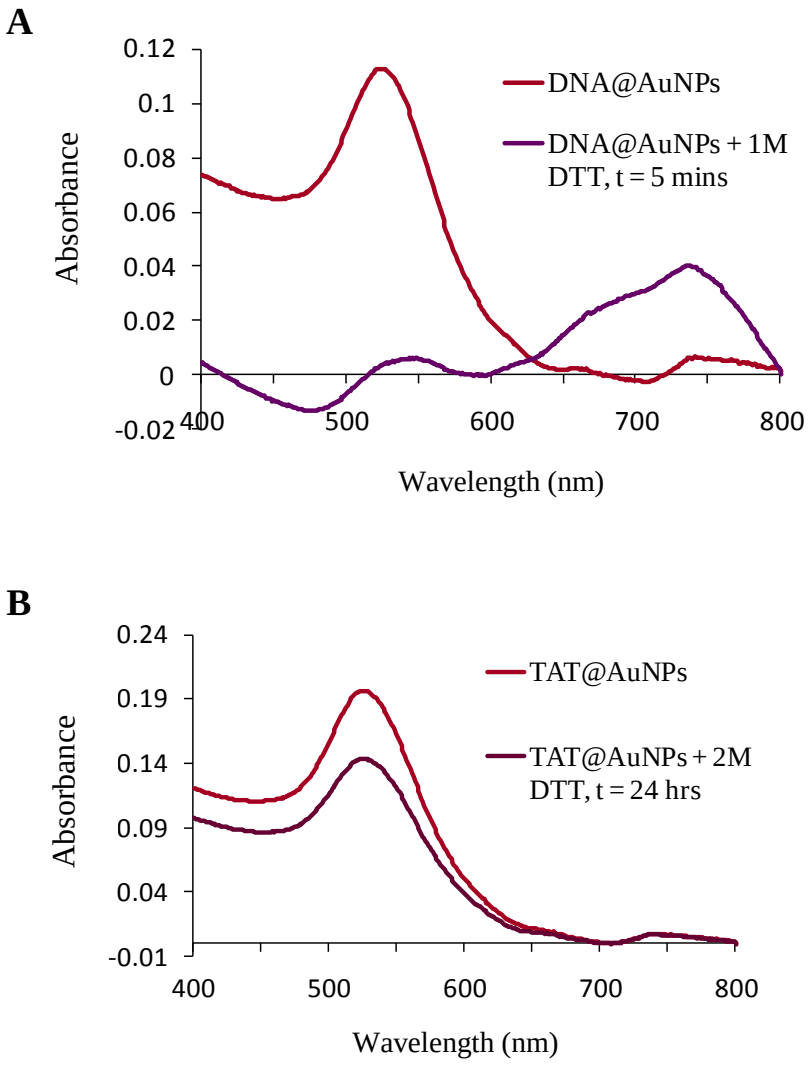

Figure 6.13 – **A** *UV-vis spectra showing gold nanoparticle aggregation on addition of DTT to DNA@AuNPs, as indicated by weak absorbance and a red-shift in* λ_{max} *towards 700 nm;* **B** *UV-vis spectra showing gold nanoparticle stability on addition of DTT to* $(PEG)_{41}$*@AuNPs, as indicated by the absence of a red-shift in* λ_{max}

As a result of these findings, it was necessary to find an alternative method for cleavage of the labelled peptide from Tat@AuNPs. The decision was taken to attempt cleavage by enzyme hydrolysis, utilising the enzyme trypsin, which hydrolyses peptide backbones following arginine and lysine residues – residues in which Tat peptide is rich. This will bring about release of the fluorescein label through digestion of the peptide, rather than by removal of the entire peptide sequence, conjugated to the $(PEG)_{41}$ ligand. **Figure 6.14** compares the displacement and enzyme digestion methods.

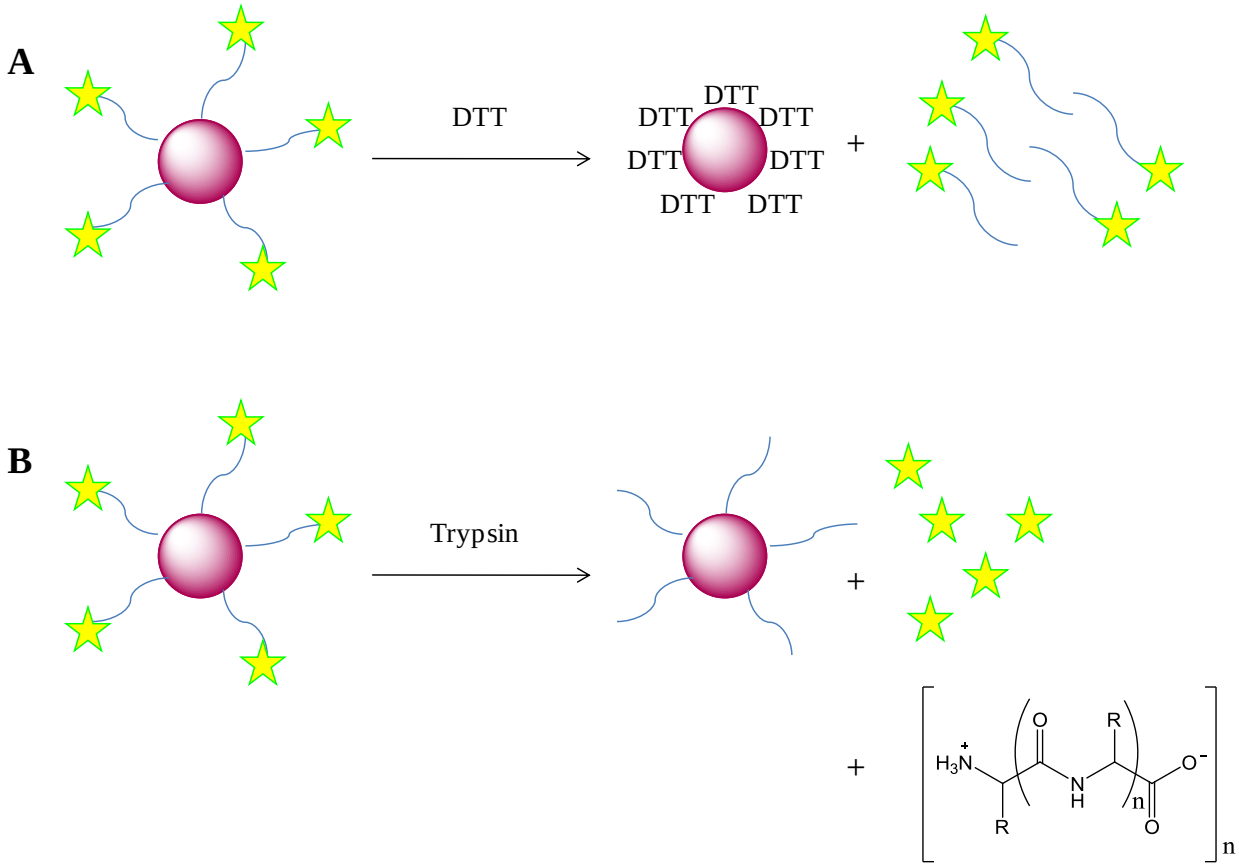

Figure 6.14 – *Schematic comparison of* **A** *Tat peptide displacement from AuNPs by disulfide reduction with DTT;* **B** *Tat peptide cleavage from AuNPs by enzyme hydrolysis with trypsin*

Samples of AuNPs were functionalised with fluorescein labelled Tat peptide as described previously to afford Tat@AuNPs. The samples were washed repeatedly in phosphate buffer (pH 7.6) until fluorescence analysis of the supernatants showed no more evidence of excess fluorescein labelled peptide. It was found that three washings were required for complete removal of unreacted peptide. Tat@AuNPs were incubated with trypsin overnight, at 37 ^{o}C. After centrifugation to separate the nanoparticles from the cleaved peptide products, the supernatants were analysed by fluorescence spectroscopy. Fluorescence was observed, thereby validating the enzyme hydrolysis method as suitable for Tat peptide quantification. [45] A numerical value for the amount of peptide conjugated to AuNPs was defined by comparison of the recorded intensity for the cleaved peptide with values on a calibration curve, composed by analysis of standard solutions of the fluorescein labelled peptide at differing concentrations. From this data it was possible to

calculate that the number of Tat peptide molecules conjugated per nanoparticle was 142.3 ± 24.5.

6.2.3 Oligonucleotide functionalisation of gold nanoparticles

Oligonucleotide functionalisation of AuNPs as a step towards the generation of an oligonucleotide nanoparticle peptide conjugate was performed using 5'- thiol modified oligonucleotide sequence (**1**), purchased from ATDBio. This sequence is functionalised at the 5'- terminus with a thiol group for surface complexation with gold and labelled at the 3'- terminus with FAM, both for quantification by fluorescence analysis and visualisation in cells.

Oligonucleotide sequence 1: 5'- AAAAAAAAAACGCATTCAGGAT (FAM) -3'

Oligonucleotide sequence (**1**) also contains of a spacer of ten adenine residues between the 5'- thiol modification and the remainder of the sequence; polyadenine spacers are used frequently in the literature and have been shown to allow effective hybridisation. [46] Polyadenine sequences have also been shown to have a greater affinity for gold surfaces than any other DNA homo-oligomer; in fact, this affinity is so great that oligo(dA).oligo(dT) hybrids have been shown to denature in the presence of a gold surface. [47]

AuNPs were functionalised with oligonucleotide sequence (**1**) using a partly modified standard protocol for oligonucleotide loading. [48] Common practice is to add DTT to solutions of thiol modified oligonucleotides before incubation with AuNPs as a way of reducing any disulfide linkages formed between the oligonucleotide strands. Prior to addition to nanoparticles HPLC size exclusion chromatography (desalting) must be performed for removal of any excess DTT and salts formed; however, this procedure can result in considerable sample losses. As such, it was decided to remove these steps from the process and add oligonucleotide sequence (**1**) to AuNPs directly. Oligonucleotide functionalisation of nanoparticles using this methodology has been shown in the literature to have no detrimental effect on the extent of oligonucleotide surface coverage. [30]

A large excess (approx. 600-fold) of oligonucleotide sequence (**1**) was added directly to citrate-reduced AuNPs, phosphate buffer was added then, as per the standard protocol, NaCl was introduced slowly, raising the concentration of salt incrementally over 48 hours. The oligonucleotide nanoparticle conjugates were then purified by centrifugation and washing to remove any unbound oligonucleotide strands. Quantification of oligonucleotide surface coverage was achieved by enzyme hydrolysis.

6.2.4 Enzyme hydrolysis vs. competitive ligand methods for quantification of oligonucleotides conjugated to gold nanoparticles

Based on the success of the enzyme hydrolysis method for quantification of Tat peptide nanoparticle conjugates, a study was undertaken to investigate the possibility of enzyme hydrolysis of oligonucleotide nanoparticle conjugates as a method for quantification and compare this method to the traditional competitive ligand method using DTT, as described previously. The enzyme chosen for this process was the endonuclease DNAse I, purchased from New England Biolabs, which nonspecifically cleaves DNA to release di-, tri- and oligonucleotide products with 5'-phosphorylated and 3'- hydroxylated ends. [50] The fluorophore of dye-labelled oligonucleotides is cleaved by the nuclease action of the enzyme. After centrifugation to remove the AuNPs, the supernatant can be analysed by fluorescence spectroscopy to determine the quantity of oligonucleotide complexed to the nanoparticle surfaces (**Fig. 6.15**).

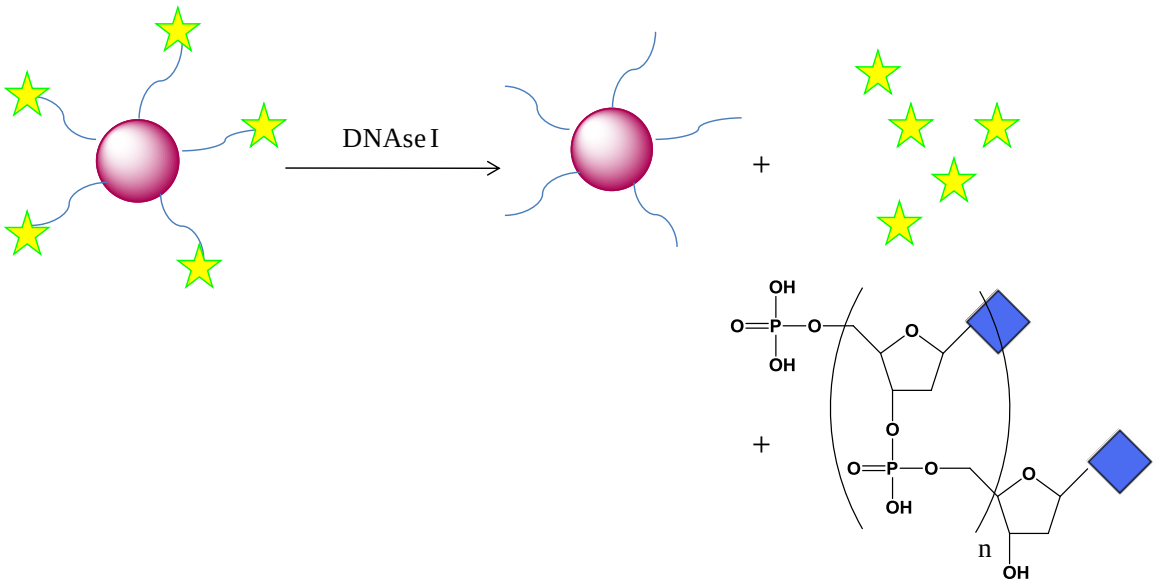

Figure 6.15 – *Schematic representation of DNA cleavage from AuNPs by enzyme hydrolysis with DNAse I*

Triplicate samples of AuNPs were functionalised with FAM labelled oligonucleotide sequence (**1**) as described previously. After centrifugation and washing to remove any unbound oligonucleotides the nanoparticles were incubated overnight with DNAse I at 37 ^{o}C. Centrifugation allowed for separation of the cleaved fluorophore from the nanoparticles, then the supernatants were analysed by fluorescence spectroscopy. Emission was observed and an average value was calculated. A calibration curve was drawn from analysis of solutions of oligonucleotide sequence (**1**) at differing concentrations. Using the average emission calculated for the cleaved fluorophore it was possible, by extrapolation of the calibration curve, to calculate the number of oligonucleotides per nanoparticle (**Table 6.2**).

In order to check that this method was viable for oligonucleotide quantification, triplicate samples of oligonucleotide nanoparticle conjugates were also treated with DTT for oligonucleotide displacement from the nanoparticle surfaces, as described by Demers *et al.* [31] Following centrifugation the supernatants were analysed by fluorescence spectroscopy. Using the calibration curve of standard concentrations, a value for the number of oligonucleotides per nanoparticle was calculated (**Table 6.2**).

Method	Number of oligonucleotides per Au nanoparticle
enzyme hydrolysis	24.52 ± 1.26
DTT displacement	24.47 ± 1.49

Table 6.2 – *Comparison of values obtained for quantification of oligonucleotides conjugated to AuNPs by enzyme hydrolysis and by DTT displacement methods*

As can be seen from the results shown in **Table 6.2**, the results for quantification of oligonucleotides conjugated to AuNPs by both enzyme hydrolysis and DTT displacement are comparable. As such, enzyme hydrolysis presents a viable alternative method to DTT displacement as a method for determination of oligonucleotide surface coverage of nanoparticles.

6.2.5 Bi-functionalisation of gold nanoparticles with oligonucleotides and $(PEG)_{41}$ ligand

With the determination of a bioconjugation method for the functionalisation of nanoparticles with Tat peptide it was now necessary to generate nanoparticles functionalised with oligonucleotide and $(PEG)_{41}$ ligand (**9**) to be used for conjugation to Tat peptide in the synthesis of an oligonucleotide nanoparticle peptide conjugate.

It was proposed that, in order to functionalise nanoparticles with both oligonucleotide and linker, the nanoparticles should first be functionalised with thiol modified oligonucleotide, followed by addition of enough $(PEG)_{41}$ ligand (**9**) to displace some, but not all, of the oligonucleotide sequences (**Fig. 6.16**). For oligonucleotide functionalisation, oligonucleotide sequence (**1**) was used. The FAM label in this sequence was used to determine oligonucleotide surface coverage post addition of the ligand by the enzyme hydrolysis method, described previously.

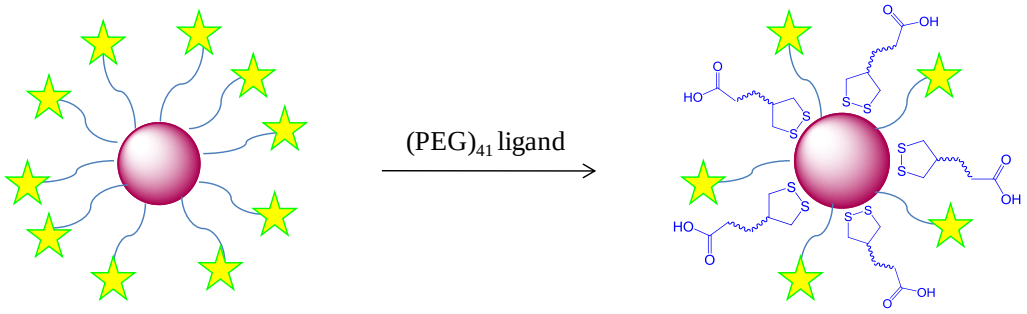

Figure 6.16 – *Bi-functionalisation of AuNPs by partial oligonucleotide displacement from oligonucleotide sequence (**1**) functionalised particles by $(PEG)_{41}$ ligand (**9**)*

A decrease in the calculated number oligonucleotide strands per nanoparticle after addition of the ligand was judged to be indicative of successful binding of the ligand to the oligonucleotide functionalised surfaces.

It was not possible to add a large excess of the $(PEG)_{41}$ ligand to oligonucleotide functionalised nanoparticles, as was the methodology used for Tat peptide functionalisation. A combination of the ligand binding to gold *via* a dithiol and its strong colloidal stabilising properties will result in it having a greater affinity for gold than the monothiol modified oligonucleotides, leading to their entire displacement from the surface and replacement with the ligand. In order to determine a feasible amount of ligand to add to avoid oligonucleotide replacement, for a rough estimate an equation determined by Mirkin *et al.* [47] was used, originally derived for calculating the amount of DNA required for functionalisation of AuNPs with a dense layer of strands:

$$\text{moles conjugated oligonucleotide} = A_n \times c_n \times D_o \times V$$

where A_n is the surface area of the nanoparticles, c_n is the concentration of the nanoparticle solution (nanoparticles per litre), D_o is the oligonucleotide density per nanoparticle (35 pmol cm^{-2} as determined by Demers *et al.* [31]) and V is the volume of nanoparticle solution (Litres). Experiments conducted for this study used 13 nm gold colloid, at a concentration of 17 nM, so the equation becomes:

$$\text{moles} = 4\pi(6.5\text{ nm})^{2} \times 17\text{ nM} \times 6.02 \times 10^{23}\text{ mol l}^{-1} \times 35\text{ pmol / cm}^{2} \times \text{L}$$

Thus the amount of $(PEG)_{41}$ ligand (**9**) required for effective 'monolayer' surface coverage of 0.5 ml samples gold colloid was calculated to be 1×10^{-9} moles. In order to find an optimum amount of ligand to add it was decided, in addition, to perform experiments using 0.5×10^{-9} moles and 2.5×10^{-9} moles ligand.

Samples of gold colloid were functionalised with FAM labelled oligonucleotide sequence (**1**) then purified of any unbound strands as described previously. Sets of triplicate samples of the oligonucleotide nanoparticle conjugates were then each incubated overnight with the three calculated amounts of $(PEG)_{41}$ ligand (**9**). After centrifugation and washing to remove any unbound ligand, the nanoparticle conjugates were treated with DNAse I, as per the enzyme assay methodology described previously, in order to determine the number of oligonucleotide strands per nanoparticle (**Table 6.3**).

The results of the DNAse I assay show that after incubation of either 0.5×10^{-9} moles or 1.0×10^{-9} moles of ligand (**9**) with oligonucleotide functionalised nanoparticles, no change in the number of oligonucleotides per particle was evident. However, incubation with 2.5×10^{-9} moles of ligand led to a decrease in the number of oligonucleotides per particle by approximately half, from 25 strands per particle to 12.5 strands per particle. This decrease was taken to be evidence that nanoparticles had been successfully bi-functionalised with both oligonucleotides and $(PEG)_{41}$ ligand, by way of partial oligonucleotide displacement by the ligand.

Number moles ligand (9) added	**Number oligonucleotides per Au nanoparticle**
0.0	24.52 ± 1.26
0.5×10^{-9}	25.16 ± 3.28
1.0×10^{-9}	25.09 ± 2.10
2.5×10^{-9}	12.51 ± 2.38

Table 6.3 – *Showing the calculated number of oligonucleotides per nanoparticle following bi-functionalisation with varying amounts of $(PEG)_{41}$ ligand (**9**)*

6.2.6 Oligonucleotide conjugation to Tat peptide *via* gold nanoparticles

Having developed a suitable methodology for functionalising AuNPs with both oligonucleotides and $(PEG)_{41}$ ligand (**9**), the final step in conjugating oligonucleotides to Tat peptide *via* AuNPs was bioconjugation of Tat peptide to the ligand molecules of the bi-functionalised particles. As described previously, bioconjugation was achieved by way of carbodiimide chemistry. However the method used previously had to be modified, with the addition of formamide to the bioconjugation mixture as a denaturant to prevent binding of Tat peptide oligonucleotide strands through ionic interactions. [49] Conjugation of Tat peptide to the oligonucleotide nanoparticle conjugates should thereby be ensured to be through the $(PEG)_{41}$ ligands only.

A possible issue with the use of formamide that had to be considered was incompatibility with gold colloid, arising from its organic nature, which could cause disruption of the stabilising layer of citrate molecules surrounding the gold particles, resulting in aggregation. AuNPs were functionalised with $(PEG)_{41}$ ligand then centrifuged and resuspended in a 1:1 mixture of phosphate buffer and formamide, but no aggregation was observed. This observation further emphasises the stabilising effect induced by the $(PEG)_{41}$ ligand; enough to prevent nanoparticle aggregation even in a highly organic environment.

A further consideration in using a high concentration of formamide as a denaturant was the possibility that hydrogen bonding with the acid functionality of the ligand could compete with the coupling reaction of the ligand and the amino side chains of Tat peptide. In order to assess whether or not this was a valid concern, before attempting Tat peptide conjugation to bi-functionalised AuNPs, conjugation to nanoparticles functionalised with ligand only, in formamide/buffer mixture, was attempted. The number of Tat peptide molecules conjugated to the nanoparticles was quantified by trypsin digestion, as described previously, and compared to the number calculated for the same conjugation reaction in the absence of formamide (**Table 6.4**).

Conjugation buffer	No. of Tat peptide molecules per Au nanoparticle
Phosphate only	142.27 ± 24.47
Phosphate/formamide (1:1)	98.99 ± 12.23

Table 6.4 – *Comparison of number of Tat peptide molecules per nanoparticle following conjugation in phosphate buffer only (pH 7.6) and phosphate/formamide (1:1) mixture (pH 7.6)*

It was found that the number of Tat peptide molecules per nanoparticle decreased by approximately 30 % in the presence of formamide. However, relatively, a significant number of peptide molecules were still conjugated to nanoparticles. As such it was decided that formamide would be suitable for use as a denaturant for Tat peptide conjugation to oligonucleotides *via* AuNPs.

Quantification of oligonucleotide surface coverage by enzyme digestion and subsequent fluorescence analysis had shown that it is possible to functionalise nanoparticles with both oligonucleotides and $(PEG)_{41}$ ligand. Similarly it was decided to use enzyme digestion as a method for determining the success of Tat peptide conjugation to the bi-functionalised nanoparticles, using fluorescence analysis to quantify the amount of fluorescein labelled Tat peptide sequence (**2**) conjugated to the nanoparticle-bound $(PEG)_{41}$ ligands.

Triplicate samples of AuNPs were first functionalised with 5'- thiol modified oligonucleotide sequence (**2**).

Oligonucleotide sequence 2: 5'- AAAAAAAAAACGCATTCAGGAT -3'

It should be noted that this sequence contains no FAM label so that any fluorescence measured following enzyme digestion resulted from fluorescein cleaved from conjugated Tat peptide only. The oligonucleotide nanoparticle conjugates were then functionalised with $(PEG)_{41}$ ligand (**9**). As determined in previous experiments, 2.5×10^{-9} moles ligand (**9**) was used for bi-functionalisation. After centrifugation and washing to remove any unbound ligand, the nanoparticle conjugates were resuspended in the phosphate/formamide (1:1) buffer. The samples were incubated

with coupling agents EDC and sulfo-NHS, before incubation fluorescein labelled Tat peptide sequence (**2**). The nanoparticle conjugates were centrifuged and washed with phosphate buffer to remove any unconjugated peptide. During washing it was observed that, on resuspending the nanoparticle conjugates in phosphate buffer, the samples were coloured blue as opposed to wine red. It was thought that this may be as a result of aggregation caused by ionic interactions between Tat peptide molecules on some nanoparticles and oligonucleotide sequences on other nanoparticles. To test this theory, formamide was added. Immediately on addition of formamide the samples returned to their original wine red colour. This observation was taken to be indicative that conjugation to Tat peptide had been successful.

Quantification of the conjugated peptide was achieved by trypsin digestion, described previously. As before, a calibration curve of fluorescence values for standard concentrations of the peptide was drawn for comparison with the fluorescence values obtained for the supernatants from the enzyme digestion. However, the average value for the number of Tat peptide molecules per nanoparticle was calculated to be 575.06 ± 53.08, approximately eight times the amount calculated for Tat peptide conjugated, in the presence of formamide, to nanoparticles functionalised with ligand only. It was thought that this anomalous result could have been caused by excess peptide molecules binding to the nanoparticle-bound oligonucleotide sequences, through ionic interactions, during the washing procedure, which took place in the absence of any denaturant. As such, conjugation was attempted again, but this time the washing procedure to remove any unconjugated peptide was performed using a 1:1 mixture of phosphate buffer and formamide. It was noted that, this time, the samples remained wine red throughout. However, following trypsin digestion, the number of peptide molecules per nanoparticle was calculated to be 579.52 ± 67.62. It was concluded that a more effective washing procedure was required to remove all unconjugated peptide in order to effectively quantify the amount of Tat peptide conjugated to the oligonucleotide nanoparticle conjugates.

Patel *et al.* [35] report the synthesis of heterofunctionalised gold nanoparticle conjugates containing both antisense oligonucleotides and synthetic peptides, including Tat peptide, using a buffer containing NaCl and the surfactant

Tween-20. It was decided to attempt Tat peptide conjugation to DNA/$(PEG)_{41}$@Au NPs using these buffer conditions. DNA/$(PEG)_{41}$@AuNPs were synthesised, as described previously. After centrifugation and washing, triplicate samples of the conjugates were resuspended in phosphate buffer, followed by introduction of Tween-20 and NaCl. The samples were activated for peptide coupling by incubation with EDC and sulfo-NHS, before addition of Tat peptide. On addition of peptide to the samples, a change in colour from wine red to blue was observed, indicating partial nanoparticle aggregation; introduction of a large excess of the highly cationic peptide had most probably disrupted the stabilising citrate layer. Formamide was added, and the samples quickly returned to red. Following incubation overnight, the samples were centrifuged then washed in a 'washing buffer' composing phosphate buffer, NaCl, Tween-20 and approximately 70 % formamide. The nanoparticle conjugates were washed several times with this buffer mixture. After each washing and centrifugation, the supernatant was analysed for fluorescence to ensure that all unconjugated peptide had been removed. With each washing a steady decrease in fluorescence was observed, indicating that this washing buffer was effective for use in purifying the nanoparticle conjugates.

Once no more fluorescence was observed in the supernatants, the conjugates were resuspended in phosphate buffer, containing 10 % formamide to prevent aggregation. However, over time, an unusual aggregation pattern was observed with apparent 'strands' of congregated red nanoparticles forming (**Fig. 6.17**).

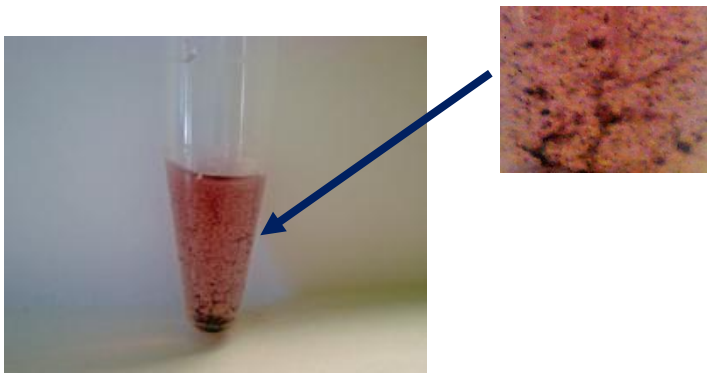

Figure 6.17 – *Images showing unusual 'strand' aggregation pattern of DNA/Tat@AuNPs suspended in phosphate/formamide (9:1) buffer*

UV-vis analysis of the triplicate samples, prior to addition of the enzyme trypsin for quantification of the conjugated peptide, showed nanoparticle aggregation over time, evident in a red-shift in λ_{max} from 525 nm to 529 nm over approximately 10 minutes. (**Fig. 6.18**). It was thought that this pattern of aggregation was induced by a degree of ionic interaction between oligonucleotides and Tat peptide molecules bound to different nanoparticles within the colloidal suspension – a possible indication of successful covalent linkage of Tat peptide to DNA/$(PEG)_{41}$@AuNPs.

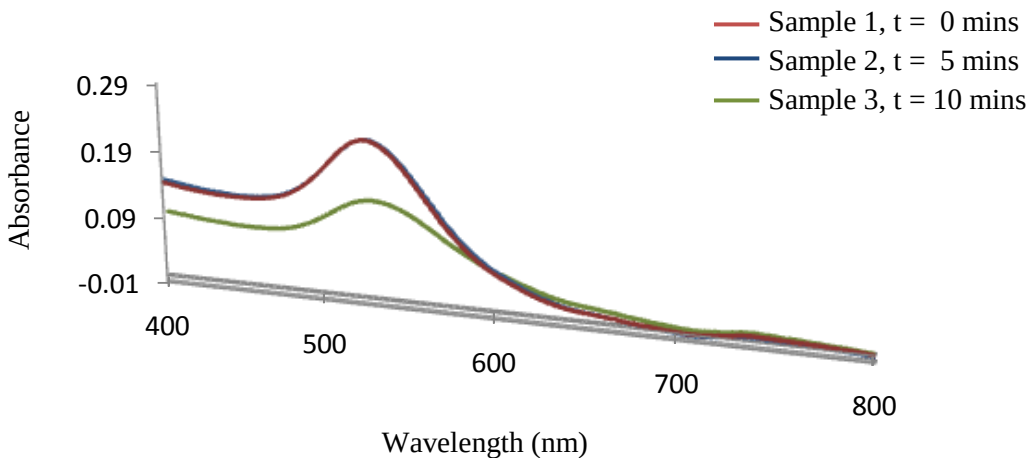

Figure 6.18 – *UV-vis spectra showing aggregation over time of DNA/Tat@AuNPs, indicated by a red-shift in the surface plasmon*

The samples were treated with trypsin for quantification of conjugated Tat peptide in the usual way. Following comparison with a calibration curve of standard peptide concentrations, the number of Tat peptide molecules per nanoparticle was calculated to be 16.02 ± 2.54. This was deemed to be a realistic quantity in view of the previous studies undertaken for conjugation of Tat peptide to $(PEG)_{41}$@AuNps (**Table 6.5**), and the fact that, with a mixed monolayer of oligonucleotide and $(PEG)_{41}$ ligand, less ligand molecules will be available for reaction with Tat peptide than when using nanoparticles functionalised with $(PEG)_{41}$ ligand only.

Functionalised nanoparticles	**Conjugation conditions**	**No. of Tat peptide molecules per nanoparticle**
$(PEG)_{41}$@AuNPs	Phosphate buffer	142.27 ± 24.47
$(PEG)_{41}$@AuNPs	Phosphate buffer / formamide (1 : 1)	98.99 ± 12.23
DNA/$(PEG)_{41}$@AuNPs	Phosphate buffer / formamide (1 : 1)	16.02 ± 2.54

Table 6.5 – *Comparison of number of Tat peptide molecules per nanoparticle conjugated to $(PEG)_{41}$@AuNPs and DNA/$(PEG)_{41}$@AuNPs*

Nanoparticle functionalisation	Particle size (nm)	Zeta potential (mV)
AuNPs	23.3	-55.1
DNA@AuNPs	43.4	-40.6
Tat@AuNPs	36.3	-22.3
DNA/Tat@AuNPs	53.9	-29.7

Table 6.6 – *Particle size and zeta potential measurements for biomolecule functionalised AuNPs c.f., bare AuNPs*

Zeta potential and particle size measurements of the heterofunctionalised nanoparticles were taken (**Table 6.6** and **Fig. 6.19**), and the values obtained compared to those obtained for nanoparticles functionalised with DNA only and nanoparticles functionalised with Tat peptide only. Zeta potential and particle size measurements for naked nanoparticles were used as a base reference.

The data shows, as expected, an increase in particle size on oligonucleotide functionalisation of AuNPs, compared with naked particles. The accompanying decrease in zeta potential is also to be expected, resulting from a decrease in charge to particle size ratio. As reported previously, nanoparticle functionalisation with Tat peptide leads to an observed increase in particle size, compared with naked particles. A significant decrease in zeta potential is also observed, thought to be due to a combination of the decrease in charge to particle size ratio and the fact that Tat peptide is rich in cationic residues, further reducing the overall particle charges.

On heterofunctionalisation of AuNPs with *both* oligonucleotides and Tat peptide, further interesting results are observed. Particle size of the nanoparticle conjugates increases compared with both DNA@AuNPs and Tat@AuNPs; this is to be expected with the increase in biomolecule functionalisation. More notable is the value obtained for zeta potential of the nanoparticle conjugates. A value of -29.7 mV was measured, which lies in the range between the values obtained for DNA@AuNPs (-40.6 mV) and Tat@AuNPs (-22.3 mV). As with the previous values obtained for functionalised nanoparticles, the decrease in zeta potential when compared to DNA@AuNPs can be partially attributed to by the overall decrease in charge to particle size ratio. However, combined with the observed increase in zeta potential

when compared to Tat@AuNPs, the value measured can also be attributed to the alteration in overall particle charge, brought about by functionalisation with both anionic oligonucleotide strands and cationic peptide molecules. As such, this data was taken as evidence to reaffirm the conclusion that oligonucleotides had been successfully conjugated to Tat peptide *via* AuNPs.

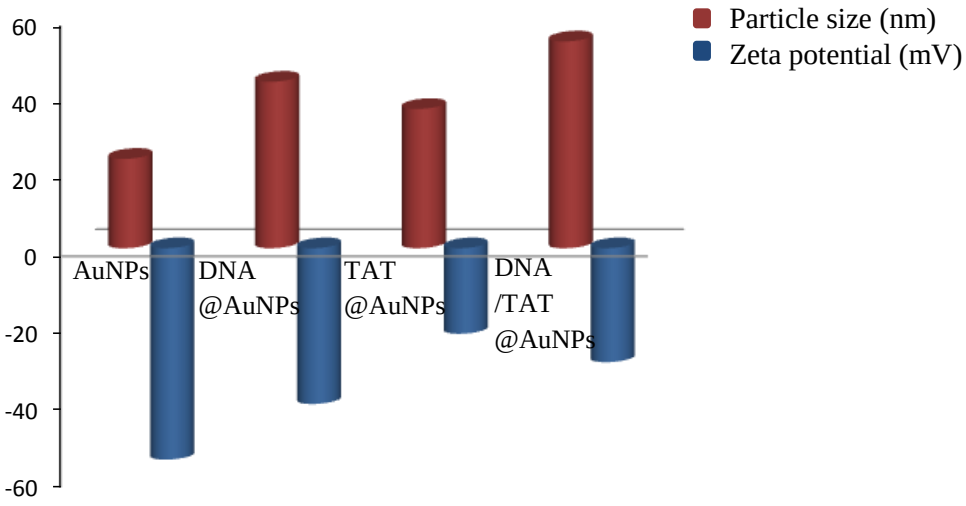

Figure 6.19 – *Graph showing comparison of particle size and zeta potential measurements for biomolecule functionalised gold nanoparticles c.f., bare AuNPs*

6.2.7 Hybridisation Studies

While conjugation of oligonucleotides to Tat peptide *via* AuNPs had been achieved successfully, in order to use these conjugations as potential biosensors their ability to hybridise with complementary oligonucleotide sequences had to be considered. In order to test this, a hybridisation study was undertaken. AuNPs were functionalised with both oligonucleotide sequence (**2**) and Tat peptide as per the methodology determined previously. AuNPs were also functionalised with complementary 5'-thiol modified oligonucleotide sequence (**3**), then a hybridisation assay was set up (**Fig. 6.20**).

Oligonucleotide sequence 3: 5'- AAAAAAAAAAATCCTGAATGCG -3'

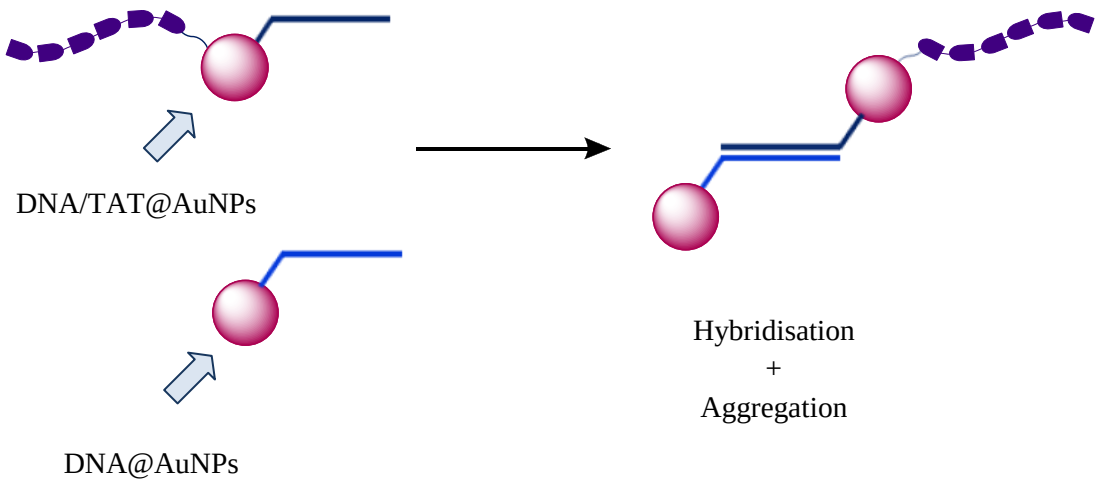

Figure 6.20 – *Schematic showing hybridisation of DNA/Tat@AuNPs to AuNPs functionalised with a complementary sequence (DNA@AuNPs) to induce nanopaticle aggregation*

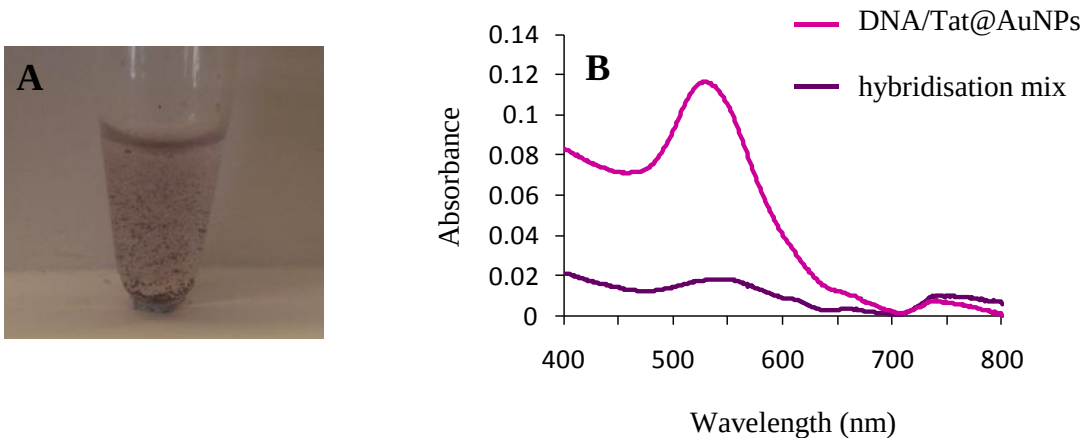

Figure 6.21 – **A** *Image showing nanoparticle aggregation following incubation of DNA/Tat@AuNPs with complementary DNA@AuNPs for 1 hour at room temperature;* **B** *UV-vis spectra showing observed decrease in absorbance of hybridisation mixture c.f., DNA/Tat@AuNPs starting material*

Complementary DNA@AuNPs were mixed with DNA/Tat@AuNPs; after incubation for 1 hour at room temperature, aggregation as a result of hybridisation of sequences **(2)** and **(3)** was visible to the naked eye (**Fig. 6.21 A**). Analysis by UV-vis spectroscopy of the hybridisation mixture showed a very weak spectrum compared with the DNA/Tat@AuNPs starting material (**Fig. 6.21 B**). The decrease

in absorbance at 535 nm was taken to be representative of aggregation by DNA hybridisation, instigating the precipitation of insoluble nanoparticle coagulates.

A control experiment was also performed by addition of nanoparticles functionalised with an oligonucleotide nonsense sequence to the DNA/Tat@AuNPs. Following incubation for 1 hour at room temperature, analysis of the mixture by UV-vis spectroscopy showed no visible decrease in absorbance at 535 nm, indicating that the aggregation observed in the previous experiment was as a result of DNA hybridisation only.

Further evidence to support this conclusion was observed in performing a DNA melt of the DNA/Tat@AuNPs hybrids. The nanoparticle aggregates were heated to 90 ^{o}C at 1 ^{o}C min^{-1}, measuring the absorbance at 535 nm. A standard sigmoidal melting curve was observed (**Fig. 6.22**) with a T_M of 61.02 ^{o}C, illustrating that the observed aggregation of the DNA/Tat@AuNPs is indeed a result of specific Watson Crick binding, since the plasmon peak is regenerated upon denaturation of the hydrogen bonds by heating.

As such, the combined data from these hybridisation studies implies that oligonucleotide conjugation to Tat peptide *via* AuNPs is a viable method for the generation of a functional DNA biosensor.

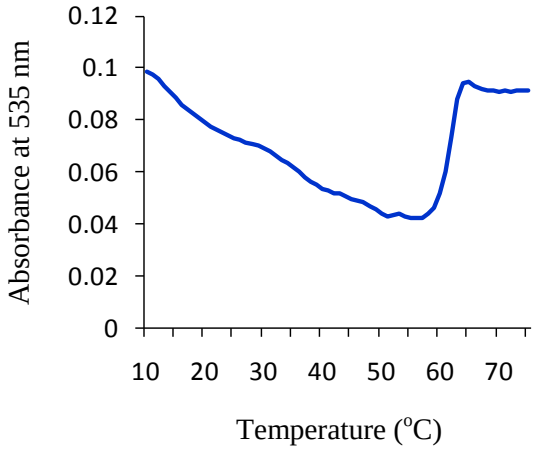

Figure 6.22 – *UV-vis spectrum showing increase in absorbance at 535 nm on 'melting' of DNA/Tat@AuNPs hybrids at 61.02 ^{o}C*

6.3 Conclusions

AuNPs have been successfully functionalised with Tat peptide. An initial approach to this, by direct addition to gold colloid of Tat peptide, containing a cysteine residue for nanoparticle adsorption, was shown to be ineffective; nanoparticle aggregation was observed, thought to be as a result of disruption of the stabilising nanoparticle citrate layers by the highly cationic peptide.

As such, a ligand for covalent attachment of Tat peptide to AuNPs was designed; this design incorporated a disulfide moiety for nanoparticle adsorption adsorption, a hydrophobic component for enhanced stability of the self-assembled monolayer, a PEG chain to impart water solubility to the functionalised nanoparticles and a carboxylic acid for ligand conjugation to Tat peptide, by coupling to the amino groups on the peptide residues. Two ligands based on this design were successfully synthesised and characterised; one ligand containing a $(PEG)_3$ chain was synthesised by solution phase chemistry and a second ligand containing a significantly longer $(PEG)_{41}$ chain was synthesised by solid phase chemistry.

AuNPs were functionalised with these ligands then Tat peptide conjugation, applying EDC/sulfo-NHS coupling chemistry, was attempted. Aggregation was observed on addition of Tat peptide to nanoparticles functionalised with the activated $(PEG)_3$ ligand; however no aggregation occured on addition of Tat peptide to the activated $(PEG)_{41}$ ligand functionalised particles. As such, the $(PEG)_{41}$ ligand was deemed suitable for use in Tat peptide conjugation to AuNPs.

Particle size and zeta potential measurements appeared to confirm successful conjugation of Tat peptide to AuNPs; an increase in particle size, accompanied with a decrease in zeta potential was indicative of this. This data was supported by development of a method for quantification of Tat peptide surface coverage, by enzyme digestion. AuNPs conjugated to fluorescein-tagged Tat peptide were treated with trypsin for cleavage by enzyme hydrolysis of the fluorescent label which was then quantified by fluorescence analysis; from the data obtained it was shown that Tat peptide surface coverage was over 100 peptides per nanoparticle.

A similar enzymatic method for quantification of oligonucleotide surface coverage of oligonucleotide-nanoparticle conjugates has been developed. A DNAse I enzyme was used to cleave FAM-labelled, thiolated oligonucleotides conjugated to AuNPs, allowing for quantification by way of fluorescence analysis of the free FAM dye. The data obtained from these experiments corroborated with data obtained using the standard DTT displacement methodology for oligonucleotide quantification. It was concluded then that enzyme hydrolysis also presents a viable alternative method to DTT displacement as a method for determination of oligonucleotide surface coverage of nanoparticles.

AuNPs have been successfully bi-functionalised with oligonucleotides and the $(PEG)_{41}$ ligand. Nanoparticles were first functionalised with oligonucleotides then an optimum amount of $(PEG)_{41}$ ligand to add, without causing oligonucleotide displacement through surface competition of the dithiol with the thiolated oligonucleotides, was determined by oligonucleotide quantification using the enzyme hydrolysis method. The optimum amount of ligand was found to be 1.0×10^{-9} moles; an amount greater than this was found to cause oligonucleotide displacement, however it was concluded that this was strong evidence of the successful binding of the ligand to the oligonucleotide functionalised surfaces.

Oligonucleotide conjugation to Tat peptide *via* AuNPs was achieved, through coupling of the peptide to the $(PEG)_{41}$ ligands of oligonucleotide / $(PEG)_{41}$ ligand functionalised nanoparticles. Particle size and zeta potential measurements confirmed this, with an increase in particle size and a more positive zeta potential observed for the Tat/DNA@AuNPs compared with the DNA/$(PEG)_{41}$@AuNPs. Hybridisation studies with both complementary and nonsense oligonucleotide sequences, and a DNA melting experiment of the aggregated nanoparticle hybrids formed as a result, confirmed the functionality of the Tat/DNA@AuNPs as potential DNA biosensors.

6.4 Experimental

6.4.1 General

For chemical synthesis, as for Chapter 2 – *Conjugation of 5'- dienyl modified oligonucleotides to Tat peptide via Diels-Alder cycloaddition.*

All reagents for gold nanoparticle synthesis were supplied by Sigma-Aldrich. Oligonucleotide sequences were supplied by ATDBio, synthesised on a 1 μmol scale and purified by HPLC. Tat peptide incorporating a cysteine residue and fluorescein labeled Tat peptide were was supplied by CSS Albachem, off resin and of > 95 % purity by HPLC analysis. Trypsin and DNAse I for enysme hydrolysis were supplied by Sigma-Aldrich and New England BioLabs respectively.

Analysis by UV-vis spectroscopy was performed on a Varian Cary 300 Bio UV-Visible spectrophotometer. Fluorescence analysis was performed on a Varian Cary Eclipse Fluorescence Spectrophotometer. Particle size and zeta potential of biomolecule functionalised AuNPs were performed on a Malvern High Performance Particle Sizer and a Malvern Zetasizer 2000 respectively.

6.4.2 Chemical synthesis

12-Hydroxy-4, 7, 10-trioxadodecanoic acid *tert*-butyl ester (2)

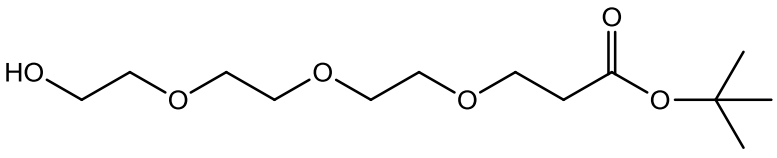

Anhydrous triethylene glycol (5 ml, 37.5 mmol) was dissolved in anhydrous THF (30 ml). Sodium metal (9 mg, 0.4 mmol) was added. The reaction mixture was stirred at room temperature until all the sodium had dissolved. *tert*-Butyl acrylate (1.8 ml, 12.4 mmol) was added. The mixture was stirred at room temperature overnight, and then quenched by addition of 1 M HCl (1 ml). The solvent was removed under reduced pressure. The residue was taken up in saturated NaCl

solution and extracted with copious EtOAc. The combined organic phases were dried over Na_2SO_4. After filtration, EtOAc was removed under reduced pressure to afford the title compound as a pale yellow liquid (3.85 g, 111 %). δ_H (400 MHz; $CDCl_3$) 1.41 (9H, s, ^{t}Bu*H*), 2.47 (2H, t, *J* 6.0, C*H*$_2$CO), 3.56 - 3.69 (14H, m, 7 x C*H*$_2$O); δ_C (100.6 MHz, $CDCl_3$) 28.1, 36.2, 61.7, 66.9, 70.3, 70.4, 70.5, 70.6, 72.6, 80.6, 171.0; *m/z* 279.1808 ([M + H$^+$] $C_{13}H_{26}O_6$ requires 279.1808).

12-Phthalimido-4, 7, 10-trioxadodecanoic acid *tert*-butyl ester (3)

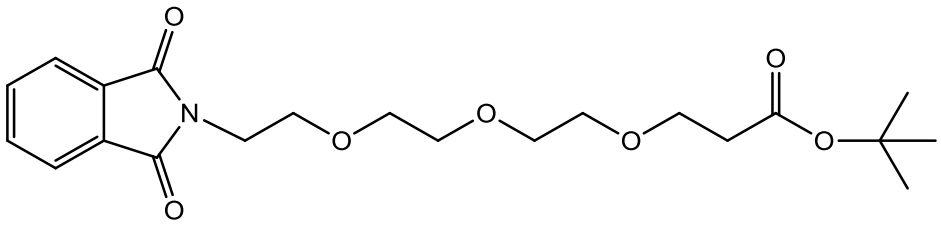

PPh_3 (5.43 g, 20.7 mmol) was dissolved in anhydrous THF (40 ml). DIAD (4 ml, 20.7 mmol) was added, under dark conditions. The reaction mixture was stirred at room temperature for 15 mins. 12-Hydroxy-4, 7, 10-trioxadodecanoic acid *tert*-butyl ester (**?**) (3.85 g, 18.8 mmol) and phthalimide (3.05 g, 20.7 mmol) were added consecutively. The mixture was stirred at room temperature overnight. The solvent was removed under reduced pressure. The residue was dissolved in EtOAc and washed with HCl solution (10 % v/v), water and saturated NaCl solution. The organic phase was dried over Na_2SO_4. After filtration, EtOAc was removed under reduced pressure to afford a yellow oil. This was washed with petroleum ether (60 ^{o}C - 80 ^{o}C) to induce precipitation of the Ph_3P=O by-product. The white solid formed was removed by filtration. Purification was by wet flash column chromatography (16 - 50 % EtOAc in petroleum ether (60 ^{o}C - 80 ^{o}C), followed by washing with a 2:1 mixture of petroleum ether (60 ^{o}C - 80 ^{o}C) and Et_2O to precipitate any co-eluting excess Ph_3P. After filtration, the solvent was removed under reduced pressure to afford the title compound as a clear oil (2.78 g, 49 %). δ_H (400 MHz, $CDCl_3$) 1.43 (9H, s, ^{t}Bu*H*), 2.47 (2H, t, *J* 6.0, C*H*$_2$CO), 3.51 - 3.74 (12H, m, 6 x C*H*$_2$O), 3.89 (2H, t, *J* 6.0, C*H*$_2$N), 7.69 - 7.71 (2H, m, Ar*H*), 7.82 - 7.84 (2H, m, Ar*H*); δ_C (100.6 MHz, $CDCl_3$) 28.2, 36.3, 37.4, 67.0, 68.0, 70.2, 70.4, 70.6, 70.7,

80.6, 123.3, 132.2, 134.0, 168.3, 171.0; *m/z* 408.2022 ([M + H^+] $C_{21}H_{29}NO_7$ requires 408.2022).

12-Amino-4, 7, 10-trioxadodecanoic acid *tert*-butyl ester **(1)**

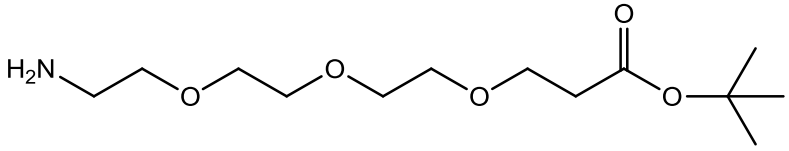

12-Phthalimido-4, 7, 10-trioxadodecanoic acid *tert*-butyl ester (**3**) (2.78 g, 6.8 mmol) was dissolved in EtOH (25 ml). $H_2N.NH_2.H_2O$ (1.3 ml, 27.2 mmol) was added. The reaction mixture was heated to reflux for 30 mins. A white precipitate formed, which was dissolved by addition of Na_2CO_3 (10 % m/v, 100 ml). The mixture was extracted with copious Et_2O. The combined organic phases were washed with water, acidified with a few drops of HCl. Solid Na_2CO_3 was added to the aqueous phase until gas evolution ceased. The aqueous phase was extracted with copious DCM. The combined organic phases were dried over Na_2SO_4. After filtration, DCM was removed under reduced pressure to afford the title compound as a yellow liquid (1.12 g, 59 %). δ_H (400 MHz; $CDCl_3$) 1.43 (9H, s, ^{t}Bu*H*), 2.48 (2H, t, *J* 6.0, C*H*$_2$O), 2.84 (2H, t, *J* 6.0, C*H*$_2$N), 3.49 (2H, t, *J* 4.0, C*H*$_2$O), 3.59 - 3.64 (8H, m, 4 x C*H*$_2$O), 3.69 (2H, t, *J* 6.0, C*H*$_2$O); δ_C (100.6 MHz, $CDCl_3$) 28.2, 36.4, 41.9, 67.1, 70.4, 70.5, 70.7, 70.7, 73.5, 80.7, 171.1; *m/z* 278.1964 ([M + H^+] $C_{13}H_{27}NO_5$ requires 278.1967).

tert-Butyl 3-(2-(5-(1, 2-dithiolan-3-yl)pentanamido)ethoxy) propanoate **(4)**

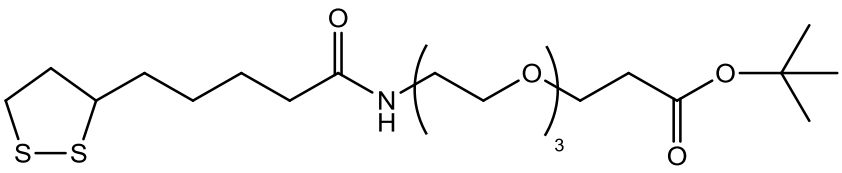

Thioctic acid (297 mg, 1.4 mmol) was dissolved in DCM. DCI (634 μl, 4.3 mmol) was added, followed by 12-amino-4, 7, 10-trioxadodecanoic acid *tert*-butyl ester (**1**) (400 mg, 1.4 mmol). The reaction mixture was stirred at room temperature

overnight. The solvent was removed under reduced pressure to afford the crude product. Purification was by wet flash column chromatography (50 - 100 % EtOAc in petroleum ether (60 ^{o}C - 80 ^{o}C) to afford the title compound as a yellow oil (408 mg, 61 %). δ_H (400 MHz, $CDCl_3$) 1.38 - 1.54 (2H, m, $CH_2CH_2CH_2$), 1.45 (9H, s, ^{t}Bu*H*), 1.63 - 1.73 (4H, m, $CH_2CH_2CH_2$), 1.88 - 1.93 (1H, m, $CHCH_2$), 2.19 (2H, t, *J* 8.0,CH_2CONH), 2.42 - 2.46 (m, 2H, CH_2CH_2S), 2.50 (2H, t, J 8.0, CH_2COO), 3.08 - 3.21 (2H, m, CH_2CH_2S), 3.45 (2H, t, *J* 6.0, CH_2O), 3.55 (2H, t, *J* 6.0, CH_2O), 3.60 - 3.66 (8H, m, 4 x CH_2O), 3.72 (2H, t, *J* 6.0, CH_2NH), 6.16 (1H, s br, N*H*); δ_C (100.6 MHz, $CDCl_3$) 23.7, 25.6, 28.3, 34.9, 36.5, 36.6, 38.7, 39.4, 40.4, 56.6, 67.1, 70.1, 70.5, 70.6, 70.7, 70.7, 80.8, 171.1, 172.9; *m/z* 466.2297 ([M + H^+] $C_{21}H_{39}NO_6S_2$ requires 466.2297).

3-(2-(5-(1, 2-Dithiolan-3-yl)pentanamido)ethoxy)propanoic acid **(5)**

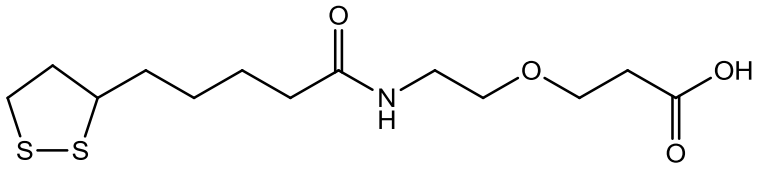

tert-Butyl 3-(2-(5-(1,2-dithiolan-3-yl)pentanamido)ethoxy)propanoate **(4)** was dissolved in DCM (3 ml). TFA (3ml) was added. The reaction mixture was stirred at room temperature for 3 hours. The solvent and TFA were removed under reduced pressure to afford a brown liquid, which was dried under reduced pressure overnight. The liquid was redissolved in DCM (5 ml). A small portion of morpholinomethyl polystyrene beads was added and the suspension was stirred at room temperature for 5 mins. The beads were removed by filtration. The solvent was removed under reduced pressure to afford the title compound as a brown oil (307 mg, 86 %). δ_H (400 MHz, $CDCl_3$) 1.39 - 1.50 (2H, m, $CH_2CH_2CH_2$), 1.59 - 1.72 (4H, m, $CH_2CH_2CH_2$), 1.86 - 1.95 (1H, m, $CHCH_2$), 1.96 - 2.05 (1H, m, CH_2CH_2S), 2.24 (2H, t, J 8.0, CH_2CONH), 2.41 - 2.52 (1H, m, CH_2CH_2S), 2.62 (2H, dt, *J* 6.0, 6.0, CH_2COO), 2.71 - 2.86 (1H, m, CH_2CH_2S), 3.08 - 3.21 (1H, m, CH_2CH_2S), 3.45 (2H, t, J 6.0, CH_2O), 3.63 - 3.67 (8H, m, 4 x CH_2O); δ_C (100.6 MHz, $CDCl_3$) 23.4, 25.9, 35.3, 35.3, 36.5, 38.8, 39.8, 40.6, 56.8, 66.9, 70.2, 70.3, 70.5, 70.7, 70.9, 174.4, 174.9; *m/z* 410.1671 ([M + H^+] $C_{17}H_{31}NO_6S_2$ requires 410.1671).

Acid functionalised resin (6)

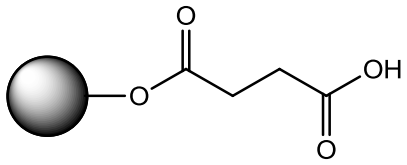

Wang resin (1.00 g, 1.0 mmol) was suspended in DCM (50 ml). Succinic anhydride (0.50 g, 5.0 mmol) and DMAP (0.60 g, 5.0 mmol) were added. The mixture was heated at 60 ^{o}C for 6 hours. The resin was isolated from the reaction mixture by filtration, and washed with MeOH (x 3) and DCM (x 3). Acid functionalisation of the resin was confirmed by suspending a sample in 0.25 % malachite green oxalate in EtOH. To this suspension was added 1 drop Et_3N. The suspension was left to stand at room temperature for 2 mins then the resin was isolated by filtration and washed with EtOH. After washing the resin remained green, confirming acid functionalisation.

Amino functionalised resin (7)

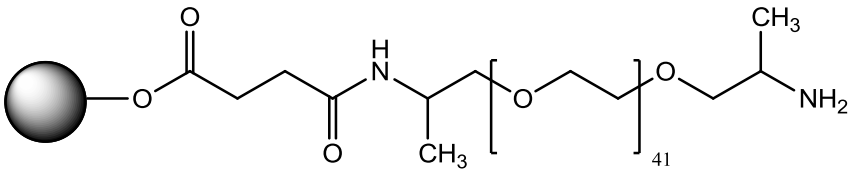

Acid functionalised Wang resin (**6**) (1.00 g, 1.0 mmol) was suspended in DCM (50 ml). Jeffamine® (9.50 g, 5.0 mmol) and DIC (775 μl, 5.0 mmol) were added. The reaction mixture was agitated at room temperature overnight. The resin was isolated from the reaction mixture by filtration and washed with MeOH (x 3) and DCM (x 3). Amino functionalisation of the resin was confirmed by the TNBS test. A sample of the resin was washed in DMF then suspended in DMF. To this suspension was added 1 drop DIPEA (10 % in DMF) and 1 drop TNBS (1 % in DMF). The suspension was left to stand at room temperature for 5 mins then the resin was isolated by filtration and washed with DMF. After washing the resin remained red-orange, confirming amino functionalisation.

Dithiol functionalised resin (8)

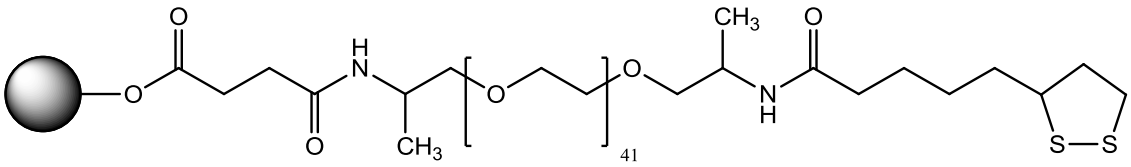

Amino functionalised Wang resin (**7**) (0.50 g, 0.5 mmol) was suspended in DCM (50 ml). Thioctic acid (516 mg, 2.5 mmol) and DIC (387 μl, 2.5 mmol) were added. The mixture was agitated at room temperature overnight. The resin was isolated from the reaction mixture by filtration and washed with MeOH (x 3) and DCM (x 3).

19-(1, 2-Dithiolan-3-yl)-6, 13-dimethyl-4, 15-dioxo-8, 11-dioxa-5, 14-diazanonadecan-1-oic acid (9)

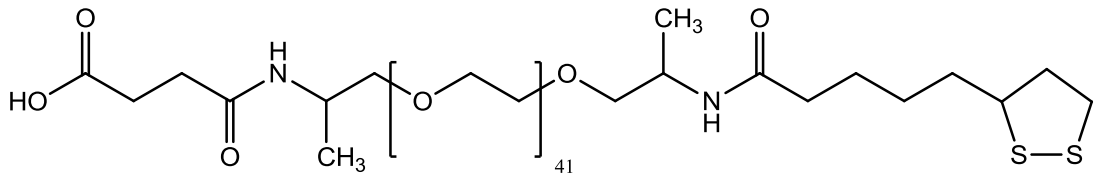

Disulfide functionalised Wang resin (0.50 g, 0.5 mmol) was suspended in DCM (9 ml). To this suspension was added TFA (1 ml). The reaction mixture was agitated at room temperature for 3 hours. The cleaved acid was isolated from the resin by filtration. The solvent and TFA were removed under reduced pressure. The yellow residual oil was dried under reduced pressure, overnight. The oil was washed with Et_2O. The solvent was removed by decantation and the oil was dried again under reduced pressure, overnight, to afford the title compound in the form of a pale yellow oil (283 mg, 13 %). MALDI-TOF: $C_{100}H_{195}O_{46}N_2$ requires ~2188; found 2086.6 ± 346.9.

6.4.2 Synthesis of citrate-reduced gold nano-particles (13 nm diameter)

To distilled water (500 ml) was added sodium tetrachloroaurate (III) dihydrate (50 mg, 0.1 mmol). The solution was heated to boiling then a solution of sodium citrate (0.075 g, 0.3 mmol) in distilled water (2.5 ml) was added. The mixture was allowed to boil for 15 mins, during which time a colour change from black to ruby-red was observed, then allowed to cool. The colloidal suspension was concentrated by centrifugation at 5000 rpm for 2 hours.

6.4.3 $(PEG)_n$ ligand functionalisation of gold nanoparticles

6.4.3.1 Generation of $(PEG)_3$@AuNPs

To three replicate samples of citrate - reduced nanoparticles (1 ml, 17 nM) was added linker (**9**) (1×10^{-7} moles of a MeOH solution). The samples were incubated at room temperature overnight then centrifuged at 7000 rpm for 20 mins. The nanoparticles were resuspended in Milli-Q water (1 ml). This was repeated twice. The samples were centrifuged once more then resuspended in phosphate buffer (960 μl, 10 mM, pH 7.6).

6.4.3.2 Generation of $(PEG)_{41}$@AuNPs

To three replicate samples of citrate - reduced nanoparticles (1 ml, 17 nM) was added linker (**9**) (1×10^{-7} moles of an aqueous solution). The samples were incubated at room temperature overnight then centrifuged at 7000 rpm for 20 mins. The functionalized nanoparticles were resuspended in Milli-Q water (1 ml). This washing procedure was repeated twice. The samples were centrifuged once more then resuspended in phosphate buffer (960 μl, 10 mM, pH 7.6).

6.4.4 Bioconjugation of Tat peptide to gold nanoparticles

6.4.4.1 Generation of Tat@AuNPs

To three replicate samples of $(PEG)_{41}$ functionalised nanoparticles (960 μl, 18 nM) in phosphate buffer (10 mM, pH 7.6) was added 20 μl EDC (2 mg ml^{-1}) and 20 μl sulfo-NHS (2 mg ml^{-1}). The samples were incubated at room temperature for 30 mins, then fluorescein labelled Tat peptide was added (1 x 10^{-8} moles of a methanol solution). The samples were incubated at room temperature overnight then centrifuged at 7000 rpm for 20 mins. The functionalised nanoparticles were resuspended in phosphate buffer (1 ml, 10 mM, pH 7.6). This washing procedure was repeated three times. The samples were centrifuged once more then resuspended in phosphate buffer (650 μl, 10 mM, pH 7.6). The samples were analysed by UV-vis spectroscopy to determine the concentration of nanoparticles, using a molar extinction coefficient of 2.7 x 10^8 M^{-1} cm^{-1}.

6.4.4.2 Quantification of Tat peptide in Tat@AuNPs by enzyme hydrolysis

To three replicate samples of AuNPs functionalised with fluorescein labelled Tat peptide (640 μl, 8 nM), in phosphate buffer (10 mM, pH 7.6), or phosphate buffer and formamide (1:1, 10mM phosphate, pH 7.6) was added trypsin (160 μl, 1 mg ml^{-1} in phosphate buffer (10 mM, pH 7.6)). The samples were incubated at 37 ^oC, overnight then centrifuged at 7000 rpm for 20 mins. The supernatant was extracted and analysed for fluorescence using an excitation wavelength of 494 nm. The concentration of fluorescein label in the supernatant was determined using a calibration graph of standard solutions. The number of Tat peptide molecules per nanoparticle was calculated by evaluating the concentration of fluorescein against the concentration of nanoparticles, calculated from the UV-vis spectroscopy data taken previously.

6.4.5 Oligonucleotide functionalisation of gold nanoparticles

6.4.5.1 Generation of DNA@AuNPs

To three replicate samples of citrate-reduced nanoparticles (1 ml, 17 nM) was added oligonucleotide sequence (**1**) (1 x 10^{-8} moles). Phosphate buffer (60 mM, pH 7.6) was added to a final concentration of 10 mM. The samples were incubated at room temperature overnight then NaCl (2 M) was added over a period of 48 hours to a final concentration of 0.1 M. The samples were centrifuged at 7000 rpm for 20 mins and the nanoparticles were resuspended in phosphate buffer (1 ml, 10 mM, pH 7.6). This washing procedure was repeated three times. The samples were centrifuged once more then resuspended in 770 μl DNAse I reaction buffer (10 mM Tris-HCl, 2.5 mM $MgCl_2$, 0.5 mM $CaCl_2$, pH 7.6). The samples were analysed by UV-vis spectroscopy to determine the concentration of nanoparticles, using a molar extinction coefficient of 2.7 x 10^8 M^{-1} cm^{-1}.

6.4.5.2 Quantification of oligonucleotides in DNA@AuNPs by DTT displacement

To three replicate samples of AuNPs functionalised with FAM labelled oligonucleotide sequence (**1**) (900 μl, 24 nM), in NaCl (0.3 M) and phosphate buffer (pH 7.6, 10mM), was added DTT (100 μ1, 1 M). The samples were incubated at room temperature, overnight then centrifuged at 7000 rpm for 20 mins. The supernatant was extracted and analysed for fluorescence using an excitation wavelength of 494 nm. The concentration of FAM label in the supernatant was determined using a calibration graph of standard solutions. The number of DNA molecules per nanoparticle was calculated by evaluating the calculated concentration of FAM against the concentration of nanoparticles, calculated from the UV-vis spectroscopy data taken previously.

6.4.5.3 Quantification of oligonucleotides in DNA@AuNPs by enzyme hydrolysis

To three replicate samples of AuNPs functionalised with FAM labelled oligonucleotide sequence (**1**) (750 μl, 29 nM), in DNAse I reaction buffer (10 mM Tris-HCl, 2.5 mM $MgCl_2$, 0.5 mM $CaCl_2$, pH 7.6), was added 50 μl DNAse I. The samples were incubated at 37 ^oC, overnight then centrifuged at 7000 rpm for 20 mins. The supernatant was extracted and analysed for fluorescence using an excitation wavelength of 494 nm. The concentration of FAM label in the supernatant was determined using a calibration graph of standard solutions. The number of DNA molecules per nanoparticle was calculated by evaluating the calculated concentration of FAM against the concentration of nanoparticles, calculated from the UV-vis spectroscopy data taken previously.

6.4.6 Bi-functionalisation of gold nanoparticles with oligonucleotides and $(PEG)_{41}$ ligand

6.4.6.1 Generation of DNA/$(PEG)_{41}$@AuNPs

To nine replicate samples of citrate-reduced nanoparticles (500 μl, 17 nM) was added oligonucleotide sequence (**1**) (0.5×10^{-8} moles). Phosphate buffer (60 mM, pH 7.6) was added to a final concentration of 10 mM. The samples were incubated at room temperature overnight then NaCl (2 M) was added over a period of 48 hours to a final concentration of 0.1 M. The samples were centrifuged at 7000 rpm for 20 mins and the nanoparticles were resuspended in phosphate buffer (500 μl, 10 mM, pH 7.6). The samples were centrifuged at 7000 rpm for 20 mins and the nanoparticles were resuspended in phosphate buffer (500 μl, 10 mM, pH 7.6). This washing procedure was repeated three times. To sets of three replicate samples of the DNA functionalised nanoparticles were added differing amounts of linker (**9**) (0.5×10^{-9} moles, 1×10^{-9} moles and 2.5×10^{-9} moles of an aqueous solution). The samples were incubated at room temperature overnight then centrifuged at 7000 rpm for 20 mins. The functionalised nanoparticles were resuspended in phosphate buffer (500 μl, 10 mM, pH 7.6). This washing procedure was repeated twice. The samples

were centrifuged once more then resuspended in 385 μl DNAse I reaction buffer (10 mM Tris-HCl, 2.5 mM $MgCl_2$, 0.5 mM $CaCl_2$, pH 7.6). The samples were analysed by UV-vis spectroscopy to determine the concentration of nanoparticles, using a molar extinction coefficient of 2.7×10^8 M^{-1} cm^{-1}.

6.4.6.2 Quantification of oligonucleotides in DNA/$(PEG)_{41}$@AuNPs by enzyme hydrolysis

To three replicate samples of AuNPs functionalised with FAM labelled oligonucleotide sequence (**1**) (375 μl, 16 nM), in DNAse I reaction buffer (10 mM Tris-HCl, 2.5 mM $MgCl_2$, 0.5 mM $CaCl_2$, pH 7.6), was added 25 μl DNAse I. The samples were incubated at 37 ^oC, overnight then centrifuged at 7000 rpm for 20 mins. The supernatant was extracted and analysed for fluorescence using an excitation wavelength of 494 nm. The concentration of FAM label in the supernatant was determined using a calibration graph of standard solutions. The number of DNA molecules per nanoparticle was calculated by evaluating the concentration of FAM against the concentration of nanoparticles, calculated from the UV-vis spectroscopy data taken previously.

6.4.7 Oligonucleotide conjugation to Tat peptide *via* gold nanoparticles

6.4.7.1 Generation of DNA/Tat@AuNPs

Sets of three replicate samples of AuNPs functionalized with oligonucleotide sequence (**2**) and 2.5×10^{-9} moles linker (**9**) were prepared as described previously. The samples were resuspended in phosphate buffer and formamide (480 μl, 1:1, 10 mM phosphate, pH 7.6) and EDC (10 μl, 2 mg ml^{-1}) and sulfo-NHS (10 μl, 2 mg ml^{-1}) were added. The samples were incubated at room temperature for 30 mins, then fluorescein labelled Tat peptide (0.5×10^{-8} moles) was added. The samples were incubated at room temperature overnight then centrifuged at 7000 rpm for 20 mins. The functionalised nanoparticles were resuspended in phosphate buffer and formamide (500 μl). This washing procedure was repeated three times. The samples

were centrifuged once more then resuspended in phosphate buffer and formamide (330 μl). The samples were analysed by UV-vis spectroscopy to determine the concentration of nanoparticles, using a molar extinction coefficient of 2.7 x 10^8 M^{-1} cm^{-1}.

6.4.7.2 Quantification of Tat peptide in DNA/Tat@AuNPs by enzyme hydrolysis

To sets of three replicate samples of AuNPs functionalised with oligonucleotide sequence (**2**) and fluorescein labelled Tat peptide (320 μl, 16 nM) in phosphate buffer and formamide (1:1, 10mM phosphate, pH 7.6), was added trypsin (80 μl, 1 mg ml^{-1} in phosphate buffer (10 mM, pH 7.6)). The samples were incubated at 37 ^oC, overnight then centrifuged at 7000 rpm for 20 mins. The supernatant was extracted and analysed for fluorescence using an excitation wavelength of 494 nm. The concentration of fluorescein label in the supernatant was determined using a calibration graph of standard solutions. The number of Tat peptide molecules per nanoparticle was calculated by evaluating the concentration of fluorescein against the concentration of nanoparticles, calculated from the UV-vis spectroscopy data taken previously.

6.4.7.3 Hybridisation Studies

To samples of DNA/Tat@AuNPs (100 μl, 4.5 nM) was added DNA@AuNps functionalized with complementary oligonucleotide sequence (**3**) (88 μl, 4.8 nM). The mixture was incubated at room temperature for 1 hour. The samples were then heated from 10 - 90 ^oC min^{-1} over 4 cycles, monitoring the absorbance at 535 nm.

6.5 References

1. Sperling, R. A., Gil, P. R., Zhang, F., Zanella, M., Parak, W. J., *Chem. Soc. Rev.*, **2008**, *37*, 1896 – 1908.
2. Patra, H. K., Banarjee, S., Chauhaudri, U., Lahiri, P., Dasgupta, A. K., *Nanomedicine*, **2007**, *3*, 111 – 119.

3. Chithrani, B. D., Ghazani, A. A., Chan, W. C. W., *Nano Lett.*, **2006**, *6*, 662 – 668.
4. Connor, E. E., Mwamuka, J., Gole, A., Murphy, C. J., Wyatt, M. D., *Small*, **2005**, *1*, 325–327.
5. Faraday, M., *Philos. Trans. R. Soc. London*, **1857**, *147*, 145 – 181.
6. Haes, A. J., Stuart, D. A., Nie, S., Van Duyne, R. P., *J. Fluoresc.*, **2004**, *14*, 355 – 367.
7. Mie, G., *Ann. Phys. Lpz.*, **1908**, *25*, 377 – 445.
8. Turkevitch, J., Garton, G., Stevenson, P. C., *J. Colloid Sci.*, **1954**, *Supplement 1*, 26 – 35.
9. Chilkoti, A., Nath, N., *J. Fluoresc.*, **2004**, *14*, 377 – 445.
10. Turkevitch, J., Stevenson, P. C., Hillier, J., *Discuss. Faraday. Soc.*, **1951**, *11*, 55 – 75.
11. Frens, G., *Nat. Phys. Sci.*, **1973**, *241*, 20 – 22.
12. Bain, C. D., Troughton, E. B., Tao, Y.-T., Evall, J., Whitesides, G. M., Nuzzo, R. G., *J. Am. Chem. Soc.*, **1989**, *111*, 321 – 335.
13. Brust, M., Walker, M., Bethell, D., Schiffrin, D. J., Whyman, R., *J. Chem. Soc., Chem. Commun.*, **1994**, 801 – 802.
14. Templeton, A. C., Wuelfing, W. P., Murray, R. W., *Acc. Chem. Res.*, **2000**, *33*, 27 – 36.
15. Kimura, K., Chen, S., *Langmuir*, **1999**, *15*, 1075 – 1082.
16. Templeton, A. C., Chen, S., Gross, S. M., Murray, R. W., *Langmuir*, **1999**, *15*, 66 – 76.
17. Wuelfing, W. P., Gross, S. M., Miles, D. T., Murray, R. W., *J. Am. Chem. Soc.*, **1998**, *120*, 12696 – 12697.
18. Bartz, M., Küther, J., Nelles, G., Weber, N., Seshadri, R., Tremel, W., *J. Mater. Chem.*, **1999**, *9*, 1121 – 1125.
19. Kanaras, A. G., Kamounah, F. S., Schaumberg, K., Kiel, C. J., Brust, M., *Chem. Comm.*, **2002**, 2294 – 2295.
20. Foos, E. E., Snow, A. W., Twigg, M. E., Ancona, M. G., *Chem. Mater.*, **2002**, *14*, 2401 – 2408.
21. Becker, C. F. W., Marsac, Y., Hazarike, P., Moser, J., Goody, R. S., Niemyer, C. M., *ChemBioChem*, **2007**, *8*, 32 – 36.

22. McKenzie, F., Ingram, A., Stokes, R., Graham, D., *Analyst*, **2009**, *134*, 549 – 556.
23. Eck, W., Craig, G., Sigdel, A., Ritter, G., Old, L. J., Tang, L., Brennan, M. F., Allen, P. J., Mason, M. D., *ACS Nano*, **2008**, *2*, 2263 – 2272.
24. Mirkin, C. A., Letsinger, R. L., Mucic, R. C., Storhoff, J. J., *Nature*, **1996**, *382*, 607 – 609.
25. Alivisatos, A. P., Johnsson, K. P., Peng, X., Wilson, T. E., Loweth, C. J., Bruchez Jr., M. P., Schultz, P. G., *Nature*, **1996**, *382*, 609 – 611.
26. Elghanian, R., Storhoff, J. J., Mucic, R. C., Letsinger, R. L., Mirkin, C. A., *Science*, **1997**, *277*, 1078 – 1081.
27. Taton, T. A., *in Current Protocols in Nucleic Acid Chemistry*, ed. Bergstrom, D. E., Glick, G. D., Jones, R. A., Beaucage, S. L., **2002**, *3*, 12.2.1 – 12.2.12, John Wiley and Sons Inc., New York.
28. Letsinger, R. L., Elghanian, R., Viswanadham, G., Mirkin, C. A., *Bioconjugate Chem.*, **2000**, *11*, 289 –291.
29. Li, Z., Jin, R., Mirkin, C. A., Letsinger, R. L., *Nucleic Acids Res.*, **2001**, *30*, 1558 – 1562.
30. Dougan, J. A., Karlsson, C., Smith, W. E., Graham, D., *Nucleic Acids Res.*, **2007**, *35*, 3668 – 3675.
31. Demers, L. M., Mirkin, C. A., Mucic, R. C., Reynolds, R.A., Letsinger, R. L., Elghanian, R., Viswanadham, G., *Anal. Chem.*, **2000**, *72*, 5535 – 5541.
32. Lewin, M., Carlesso, N., Tung, C.-H., Tang, X.-W., Cory, D., Scadden, D. T., Weissleder, R., *Nature Biotech.*, **2000**, *18*, 410 – 414.
33. de la Fuente, J. M., Berry, C., *Bioconjugate Chem.*, **2005**, *16*, 1176 – 1180.
34. Zhang, K., Fang, H., Chen, Z., Taylor, J.-S. A., Wooley, K. L., *Bioconjugate Chem.*, **2008**, *19*, 1880 – 1887.
35. Patel, P. C., Giljohann, D. A., Seferos, D. S., Mirkin, C. A., *Proc. Natl. Acad. Sci. U.S.A.*, **2008**, *105*, 17222 – 17226.
36. Marty, C., Meylan, C., Schott, H., Ballmer-Hofer, K., Schwendener, R. A., *Cell. Mol. Life. Sci.*, **2004**, *61*, 1785 – 1794.
37. Fuchs, S. M., Raines, R. T., *Cell. Mol. Life Sci.*, **2006**, *63*, 1819 – 1822.
38. Tshikudo, T. R., Wang, Z., Brust, M., *Materials Science and Technology*, **2004**, *20*, 980 – 984.

39. Seitz, O., Kunz, H., J. Org. Chem., 1997, 62, 813 – 826.
40. Hancock, W. S., Battersby, J. E., *Anal. Biochem.*, **1976**, 71, 260 – 264.
41. Hoare, D. G., Koshland, D. E., *J. Biol. Chem*., **1967**, *242*, 2447 – 2453.
42. Hermanson, G. T., in *Bioconjugate Techniques*, **1996**, 173, Elsevier, San Diego.
43. Staros, J. V., Wright, R. W., Swingle, D. M., *Anal. Biochem.*, **1986**, *156*, 220 – 222.
44. Lomant, A. J., Fairbanks, G., *J. Mol. Biol.*, **1976**, *104*, 243 – 261.
45. McKenzie, F., Steven, V., Ingram, A., Graham, D., *Chem. Comm.*, **2009**, *20*, 2872 – 2874.
46. Park, S.-J., Lazarides, A. A., Storhoff, J. J., Pesce, L., Mirkin, C. A., *J. Phys. Chem. B*, **2004**, *108*, 12375 – 12380.
47. Kimura-Suda, H., Petrovykh, D. Y., Tarlov, M. J., Whitman, L. J., *J. Am. Chem. Soc.*, **2003**, *125*, 9014–9015.
48. Storhoff, J. J., Elghanian, R., Mucic, R. C., Mirkin, C. A., Letsinger, R. L., *J. Am. Chem. Soc.*, **1998**, *120*, 1959 – 1964.
49. Turner, J. J., Ivanova, G. D., Verbeure, B., Williams, D., Arzumanov, A. A., Abes, S., Lebleu, B., Gait, M. J., *Nucleic Acids Res.*, **2005**, *33*, 6837 – 6849.
50. Kunitz, M., *J. Gen. Physiol.*, **1950**, *33*, 349 – 362.